Sensor and Simulation Notes

Note 442

March 2000

Studies of an Impulse Radiating Antenna and a Pulse Radiating Antenna Element for SAR and Target Identification Applications

Everett G. Farr and L. H. Bowen
Farr Research, Inc.

Glen R. Salo and John S. Gwynne
Mission Research Corporation

Carl E. Baum, William D. Prather, and Tyrone Tran
Air Force Research Laboratory / Directed Energy Directorate

Abstract

We have designed, built, and tested two 18-inch diameter antennas, a reflector Impulse Radiating Antenna (IRA), and a Pulse Radiating Antenna Element (PRAE). We provide extensive measurements of the two antennas, made both in the time domain range of Farr Research, and at the frequency domain range of Mission Research. We then evaluate these antennas for possible use as a lightweight component in both a Synthetic Aperture Radar (SAR) system and in a Remote Target Identification (RTID) system.

This work was sponsored in part by the Air Force Office of Scientific Research, Arlington, VA, and in part by Air Force Research Laboratory, Directed Energy Directorate, under contract # F29601-99-C-0050.

I. Introduction

We explore here the applicability of two 18-inch diameter antennas for possible application in Synthetic Aperture Radar (SAR) and Remote Target ID (RTID) systems. The two antennas considered are the Impulse Radiating Antenna (IRA) and the Pulse Radiating Antenna Element (PRAE). This work extends some of the ideas previously suggested in [1].

This note introduces the PRAE, which is a reflector IRA in which the paraboloidal reflector has been replaced by a flat plate. This substitution is made in order to broaden the antenna pattern of the IRA, which is well known to be quite narrow. Some SAR applications require a broader antenna pattern, so it was thought that the PRAE would be an interesting alternative to explore. Note, however, that we had previously looked at the beamwidth of the IRA only in the time domain, and when measured in the frequency domain, the beamwidth of the IRA does not appear to be so narrow. This is especially true at low frequencies.

We tested the antennas at two different facilities, the time domain outdoor antenna range of Farr Research, and the frequency domain anechoic chamber of Mission Research Corporation (MRC) in Dayton. There were three reasons why we tested at two facilities. First, we had never compared a set of results from each of the two measurement techniques, although we had developed expressions correlating one to the other in [2]. We can report here a very nice correlation between the time and frequency domain techniques. Second, we used the two measurement techniques because MRC was set up to take much more data automatically than the manual Farr Research antenna range. Finally, we thought that we might observe some features in the frequency domain measurements that are less obvious in the time domain measurements. This turns out to be quite true, and we will discuss the differences in the data features extensively.

We begin with a description of the antennas and the experimental data taken with both time domain and frequency domain methods. Next, we discuss the similarities and differences in the data taken two different ways. Finally, we discuss the new applications for which these antennas may be suitable, and we explore possible design improvements that will enhance their applicability to these new missions.

II. Design and Fabrication of the Antennas

We begin with the general design of the IRA, which is shown in Figure 2.1. The design of the IRA is nearly identical to that of the 18-inch Multifunction IRA (MIRA) with F/D = 0.5, which was first reported in [3] and refined in [4]. The principal difference is that there is no mechanism for an adjustable feed location; the feed point is fixed. The reflector is spun aluminum, the feed arms are copper, the resistors are the high-voltage resistors from HVR, and the support pieces near the apex are ultra-high molecular weight (UHMW) polyethylene. The splitter is the same used previously from Prodyne. A 50 Ω input is split into two 95 Ω semi-rigid 0.141 in cables.

Next, we consider the design of the PRAE, shown in Figure 2.2. The design of the PRAE is quite similar to the IRA, with the exception that the paraboloidal reflector was replaced by a flat plate. When driven by a step function, the PRAE radiates a step function or pulse on boresight at early time. On the other hand, the IRA radiates an impulse at early time. So at early time, the PRAE radiates a replica of the driving voltage, whereas an IRA radiates the derivative of the driving voltage. The distance from the focus to the plate in the PRAE is precisely the distance from the focus to the reflector along the center line of the IRA. This results in feed arm angles that are set at approximately ±45 degrees from boresight, so we expect the high-frequency beamwidths to be near ±45 degrees.

Let us consider now why we chose a diameter of 18 inches for the two antennas. We chose this diameter because such reflectors are easily available, and because they are easily shipped between the two facilities. Furthermore, there was some concern that the two test ranges may not be large enough to satisfy far-field conditions with larger antennas. To improve performance at the low frequencies, we expect that an actual device may be up to twice the diameter of the models as built. But we can easily scale the results to a larger size as required.

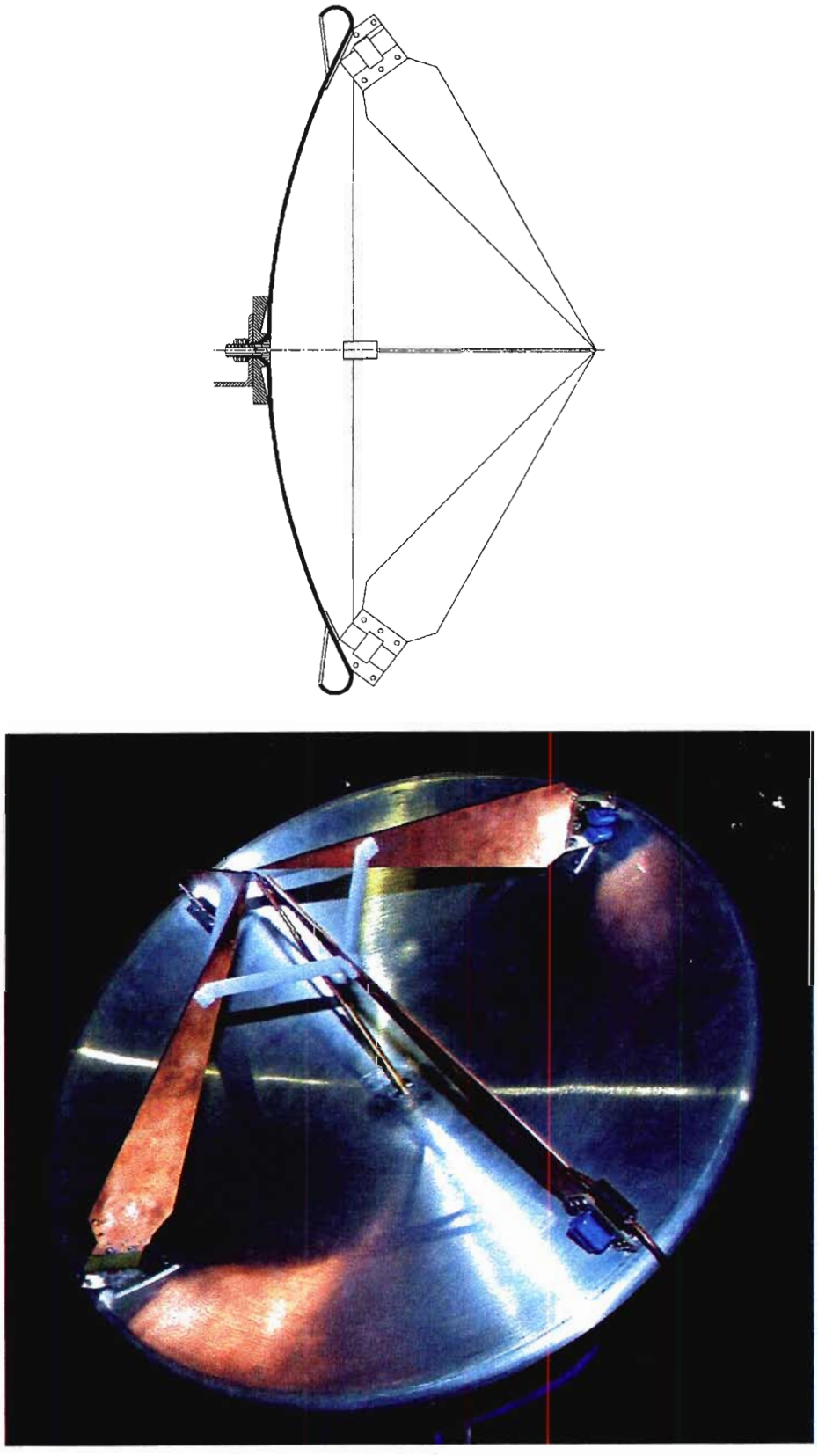

Figure 2.1 the 18-inch diameter IRA.

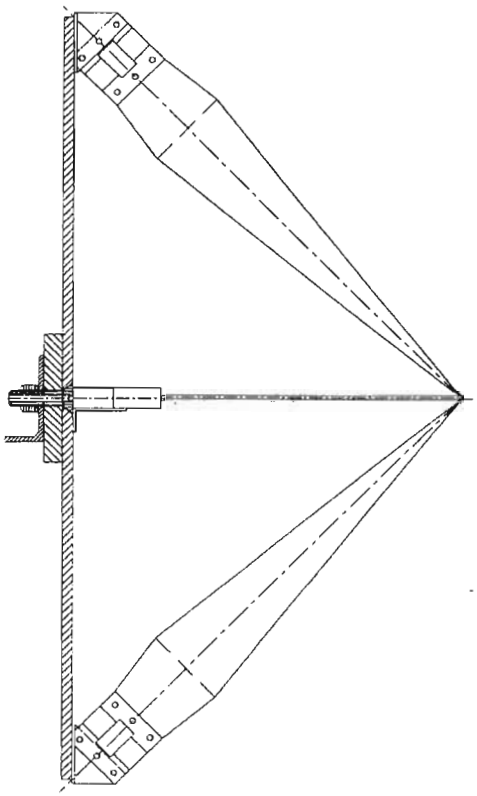

Figure 2.2 The 18-inch diameter PRAE (bottom).

III. Time Domain Measurements

Measurements were made at the Farr Research time domain antenna range at a distance of 20 meters. The source was the Picosecond Pulse Lab Model 4015C, with risetime of 20 ps and peak output of 4 V. The oscilloscope was the Tektronix 11801B, with risetime of 17 ps. The sensor was a Farr Research Model FRI-TEM-01-100 TEM horn sensor, with FWHM = 35 ps.

A. IRA Measurements

A TDR of the IRA is shown in Figure 3.1, and the raw data on boresight is shown in Figure 3.2. The normalized impulse response is shown in Figure 3.3, in both the time and frequency domains. A close-up of the time domain impulse response is shown in Figure 3.4, demonstrating a FWHM of ~75 ps. The integral of the impulse response is shown in Figure 3.5, from which we obtain h_a ~= 12 cm. This compares to an expected value of 14.9 cm, so we are measuring 81% of the expected value.

The gain for the IRA on boresight is shown in Figure 3.6. We see that the antenna is useful up to around 9 GHz. Principle plane antenna gain patterns are shown in Figures 3.7 and 3.8 for eight frequencies. Finally, pattern cuts are presented in Figure 3.9 that are based on the peak raw received voltage.

B. PRAE Measurements

A TDR of the PRAE is shown in Figure 3.10, and the raw data on boresight is shown in Figure 3.11. The normalized impulse response is shown in Figure 3.12, in both the time and frequency domains. A close-up of the time domain impulse response is shown in Figure 3.13, demonstrating a FWHM of ~315 ps. Note that this is much broader than the ~75 ps measured with the IRA, since the beam is defocused. The integral of the impulse response is shown in Figure 3.14, from which we obtain h_a ~= 10.7 cm. This compares to an expected value of 14.9 cm, so we measuring 72% of the expected value.

The gain for the PRAE on boresight is shown in Figure 3.15. We see that the antenna is useful up to around 2 GHz, which represents considerably less bandwidth than the IRA. Principle plane antenna gain patterns are shown in Figures 3.16 and 3.17 for eight frequencies. Finally, pattern cuts are presented in Figure 3.18 that are based on the peak raw received voltage.

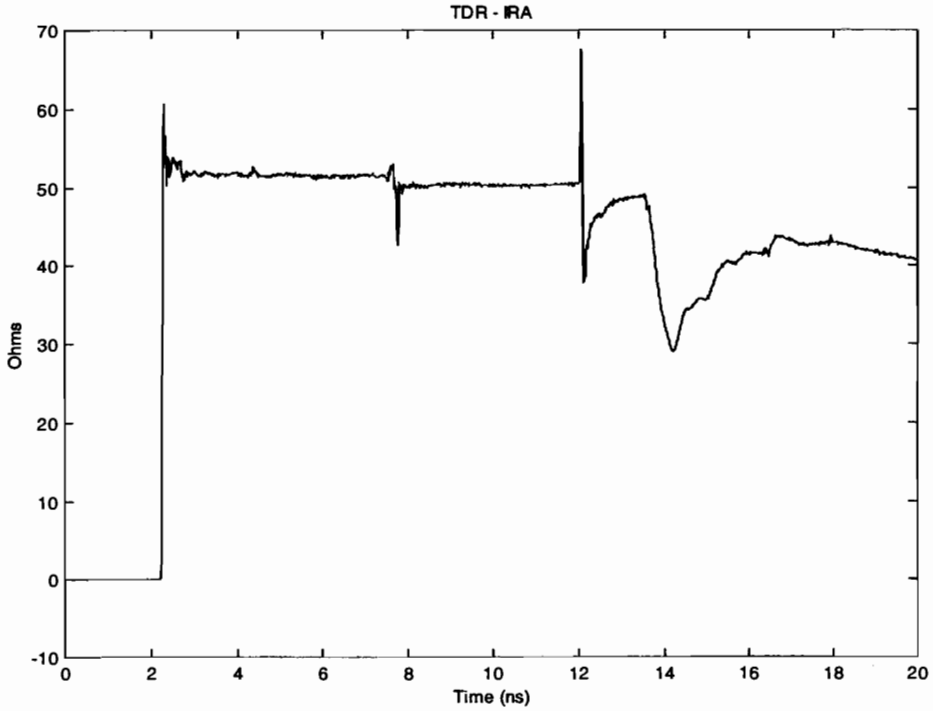

Figure 3.1 TDR of the IRA.

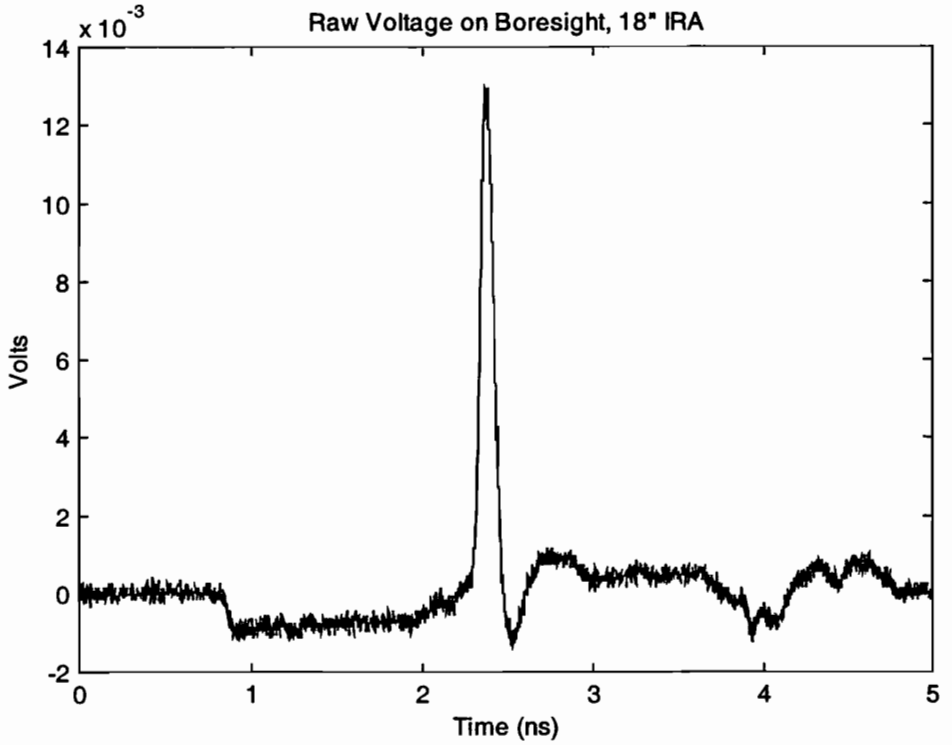

Figure 3.2 Raw waveform on boresight for the IRA.

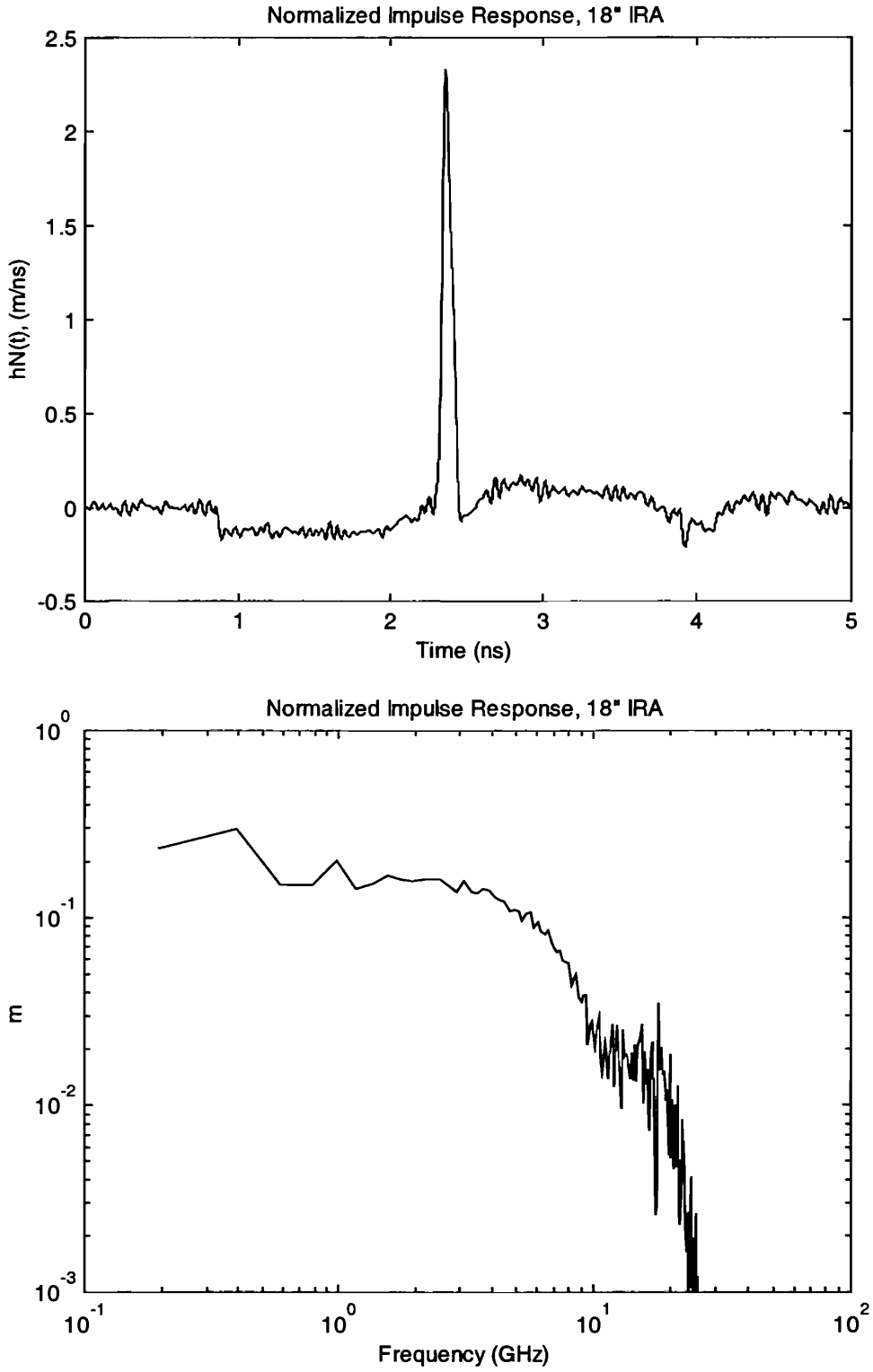

Figure 3.3. Impulse response of the IRA, in the time domain (top) and in the frequency domain (bottom).

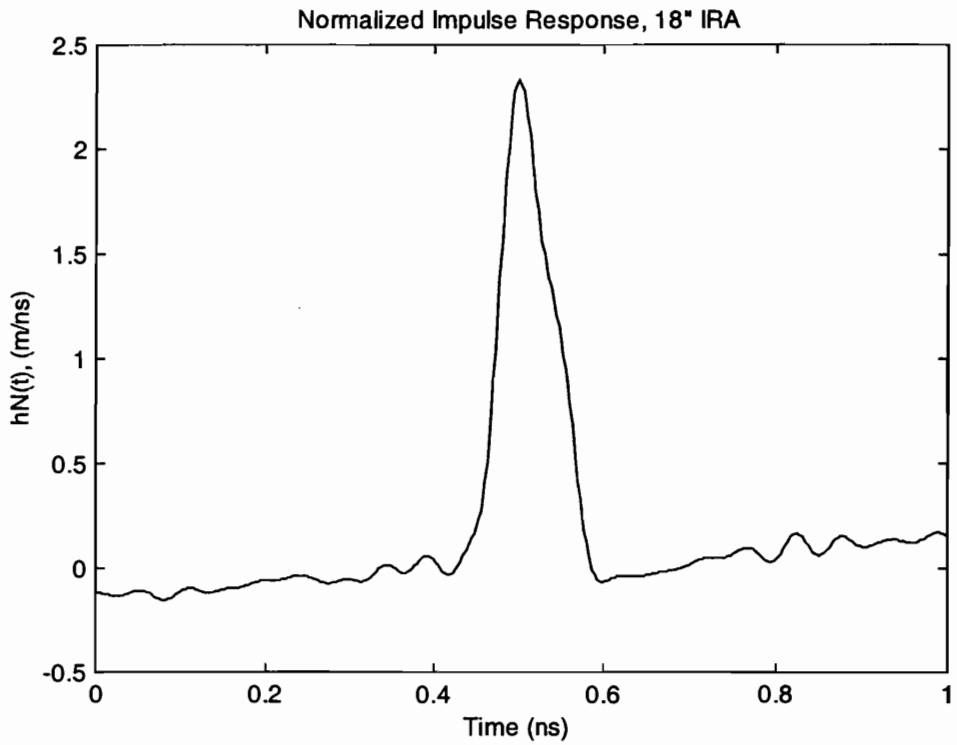

Figure 3.4. Close-up of the impulse response of the IRA.

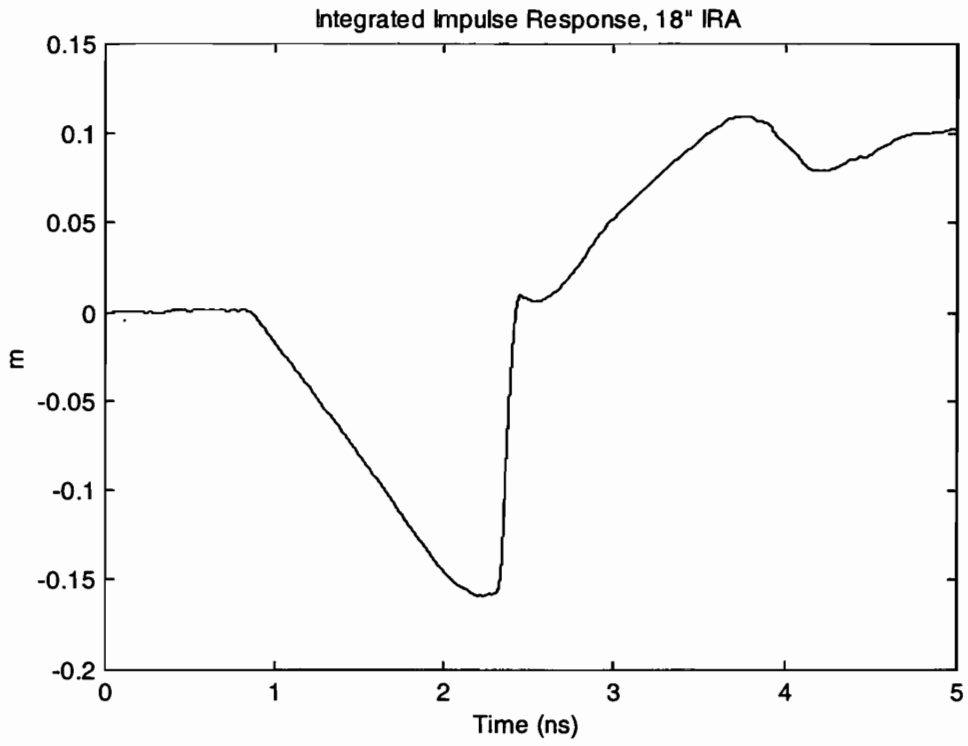

Figure 3.5 Integral of the impulse response of the IRA.

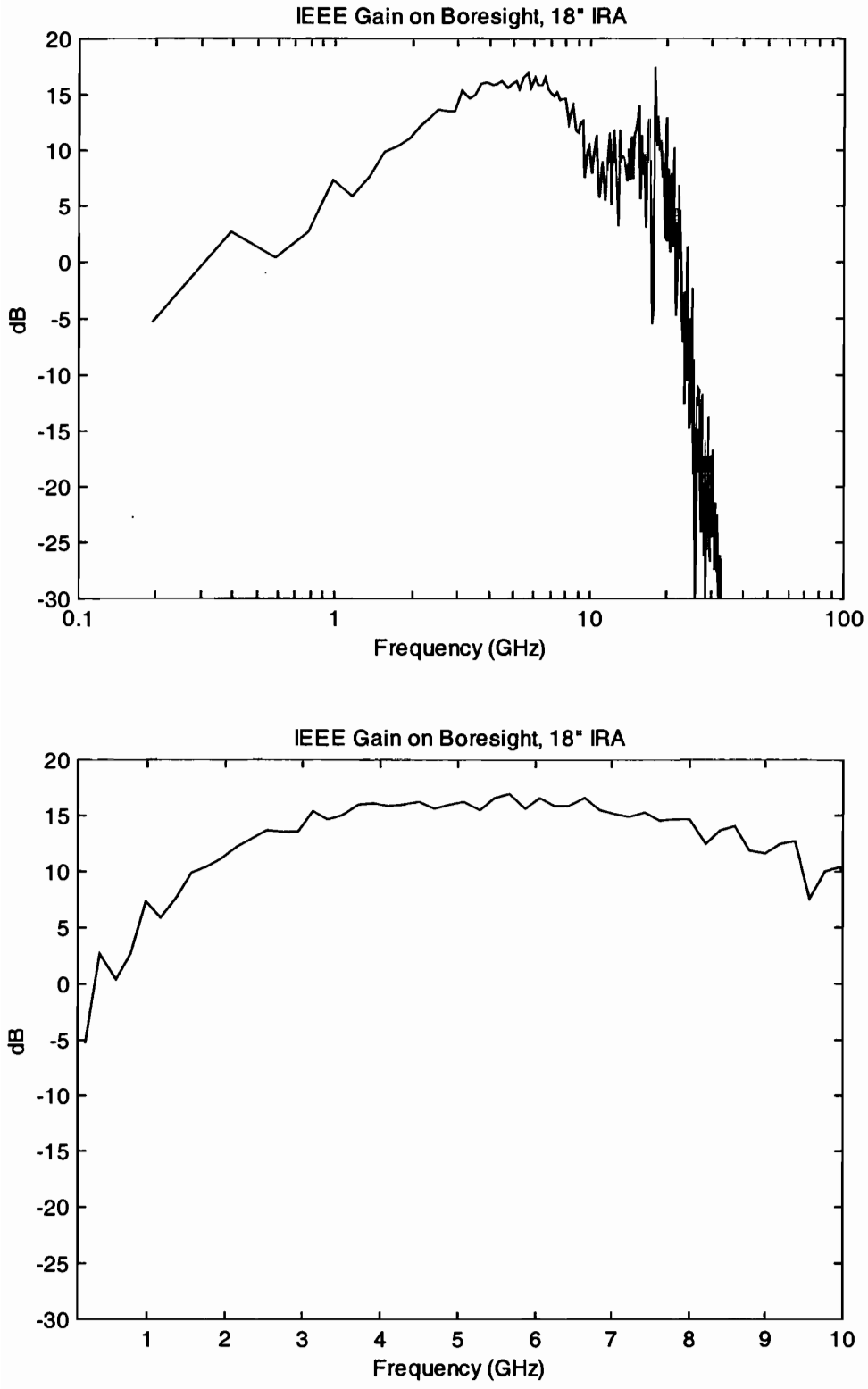

Figure 3.6. Gain of the IRA on boresight, plotted on two different scales.

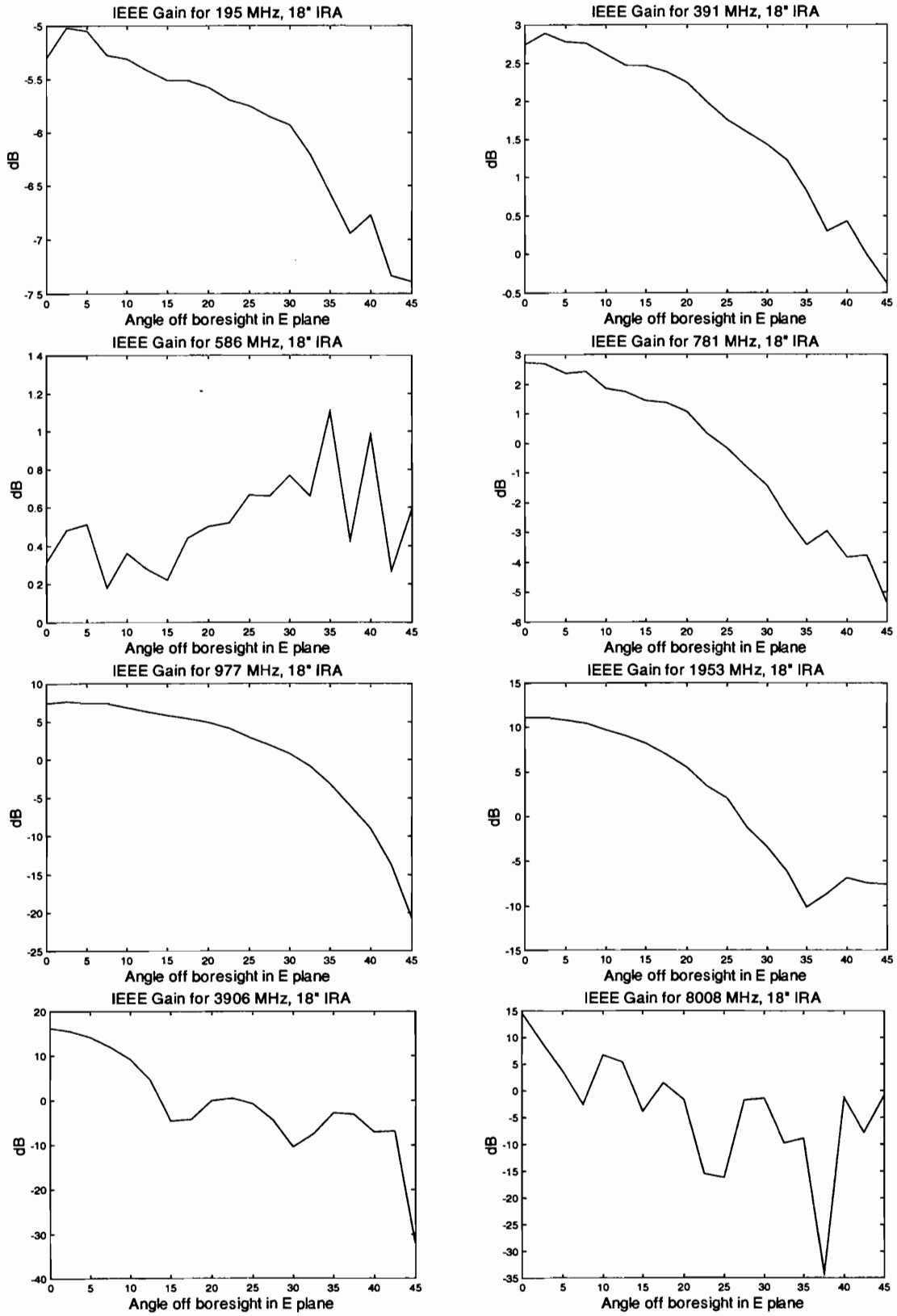

Figure 3.7. Gain of the IRA as a function of angle in the E-plane, at 195, 391, 586, 781, 977, 1953, 3906, and 8008 MHz.

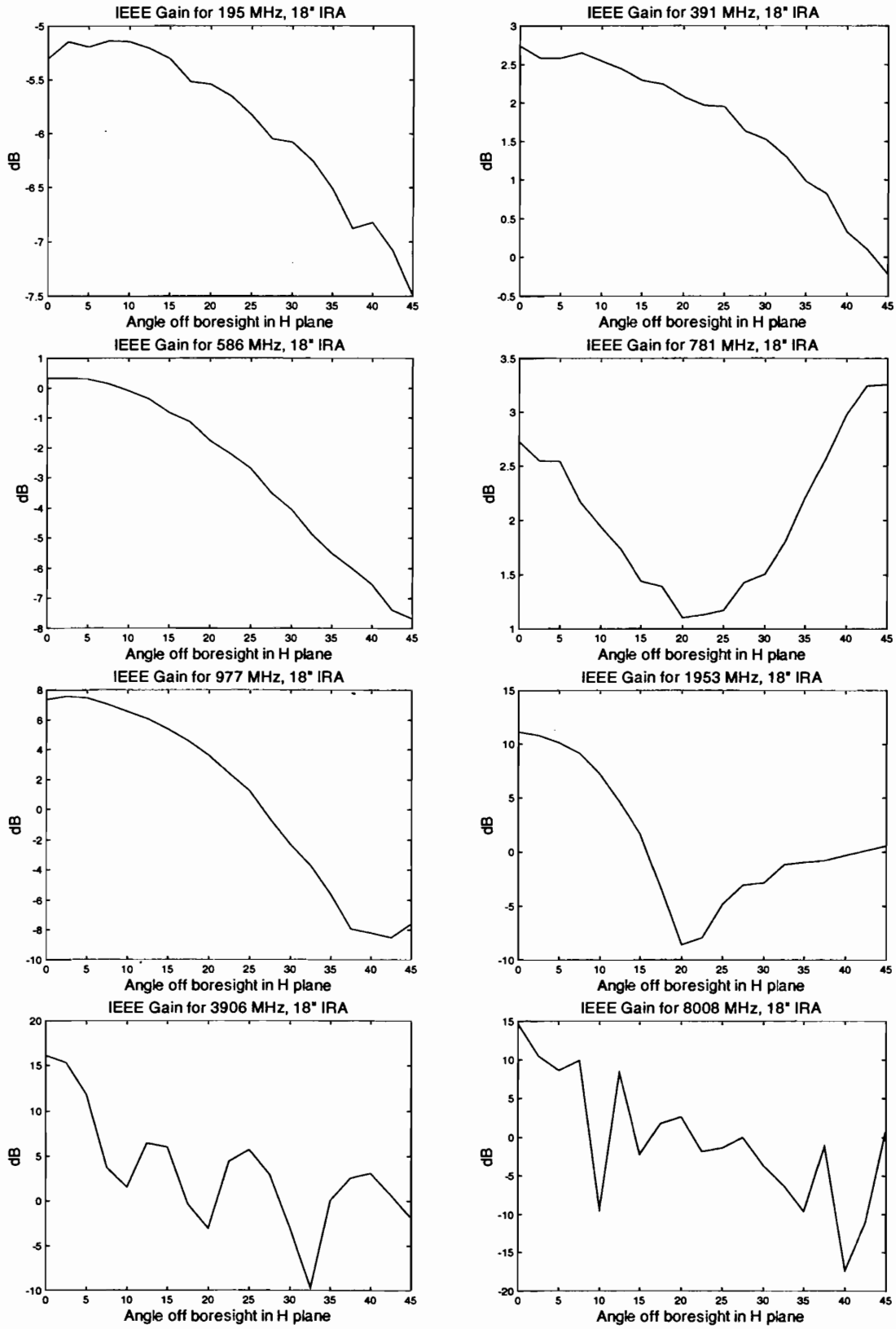

Figure 3.8. Gain of the IRA as a function of angle in the H-plane, at 195, 391, 586, 781, 977, 1953, 3906, and 8008 MHz.

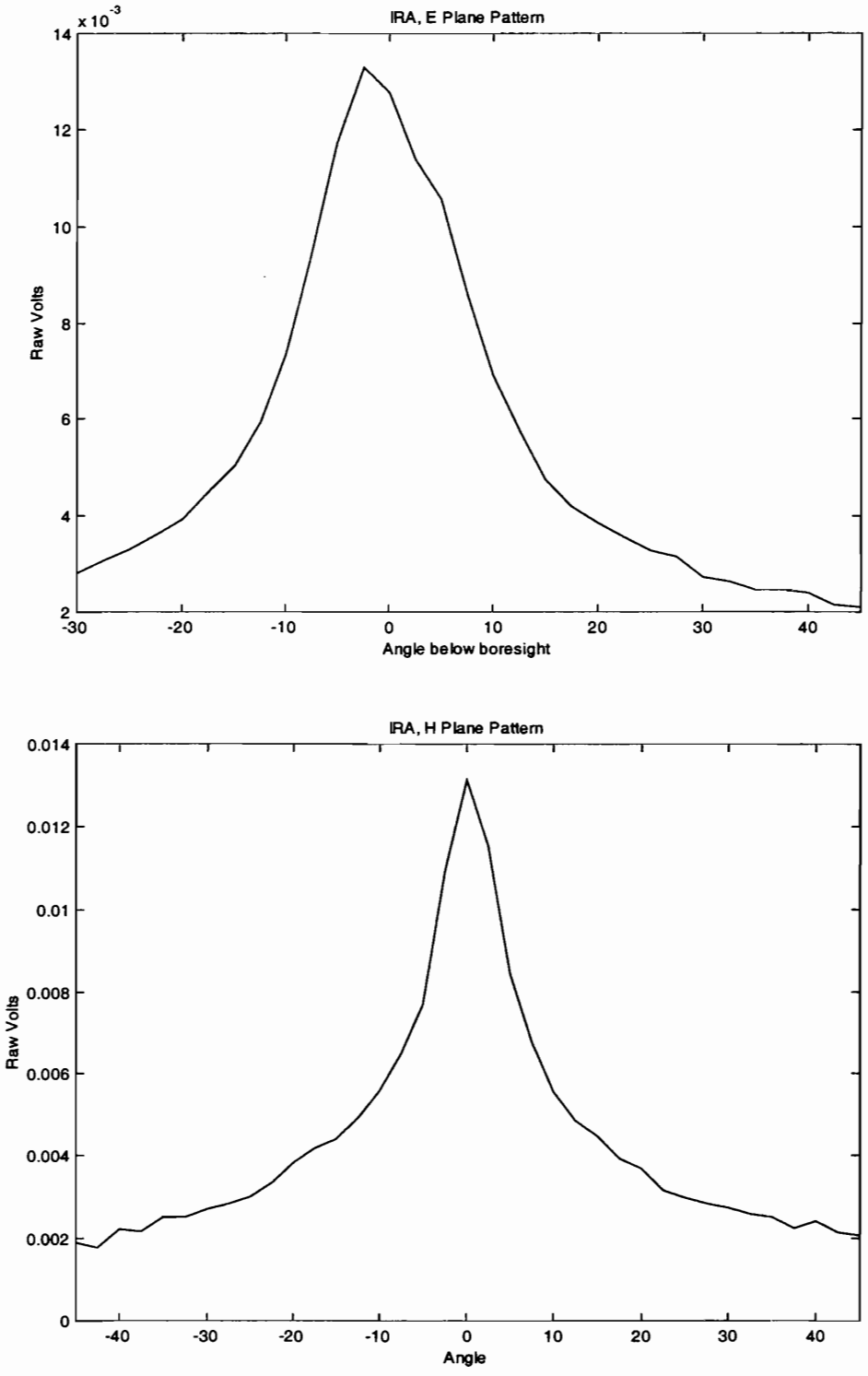

Figure 3.9. Antenna pattern in terms of peak raw voltage in the E-plane (top) and H-plane (bottom).

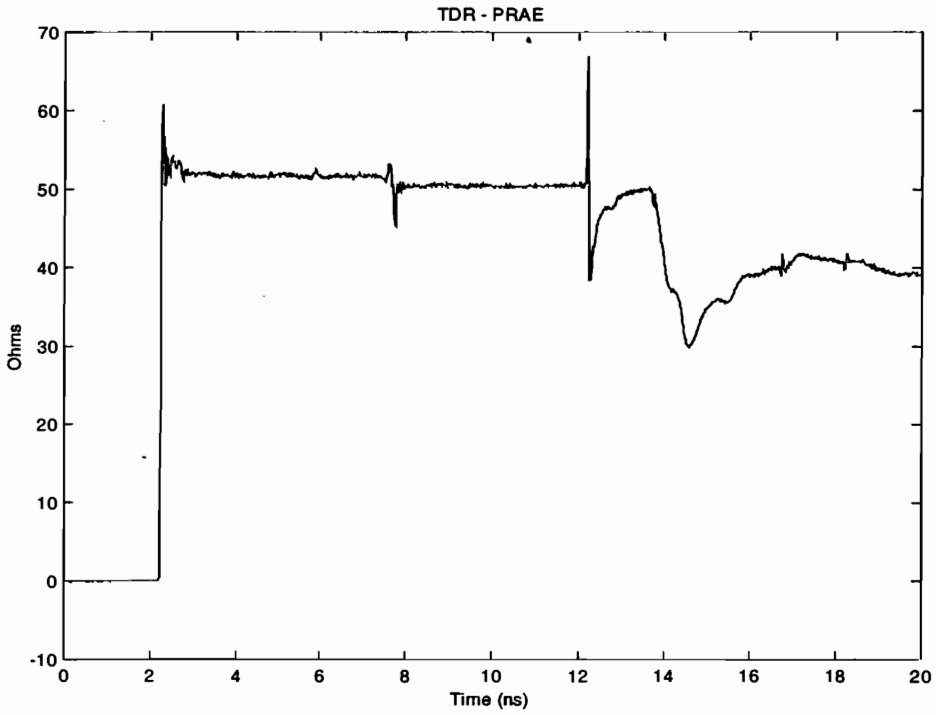

Figure 3.10 TDR of the PRAE.

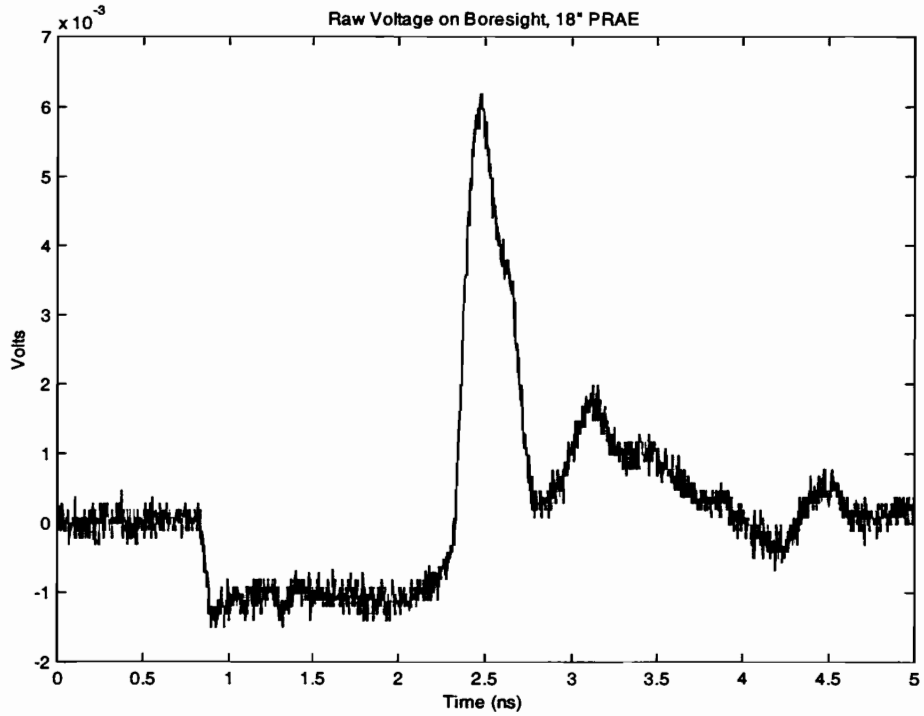

Figure 3.11. Raw waveform on boresight for the PRAE.

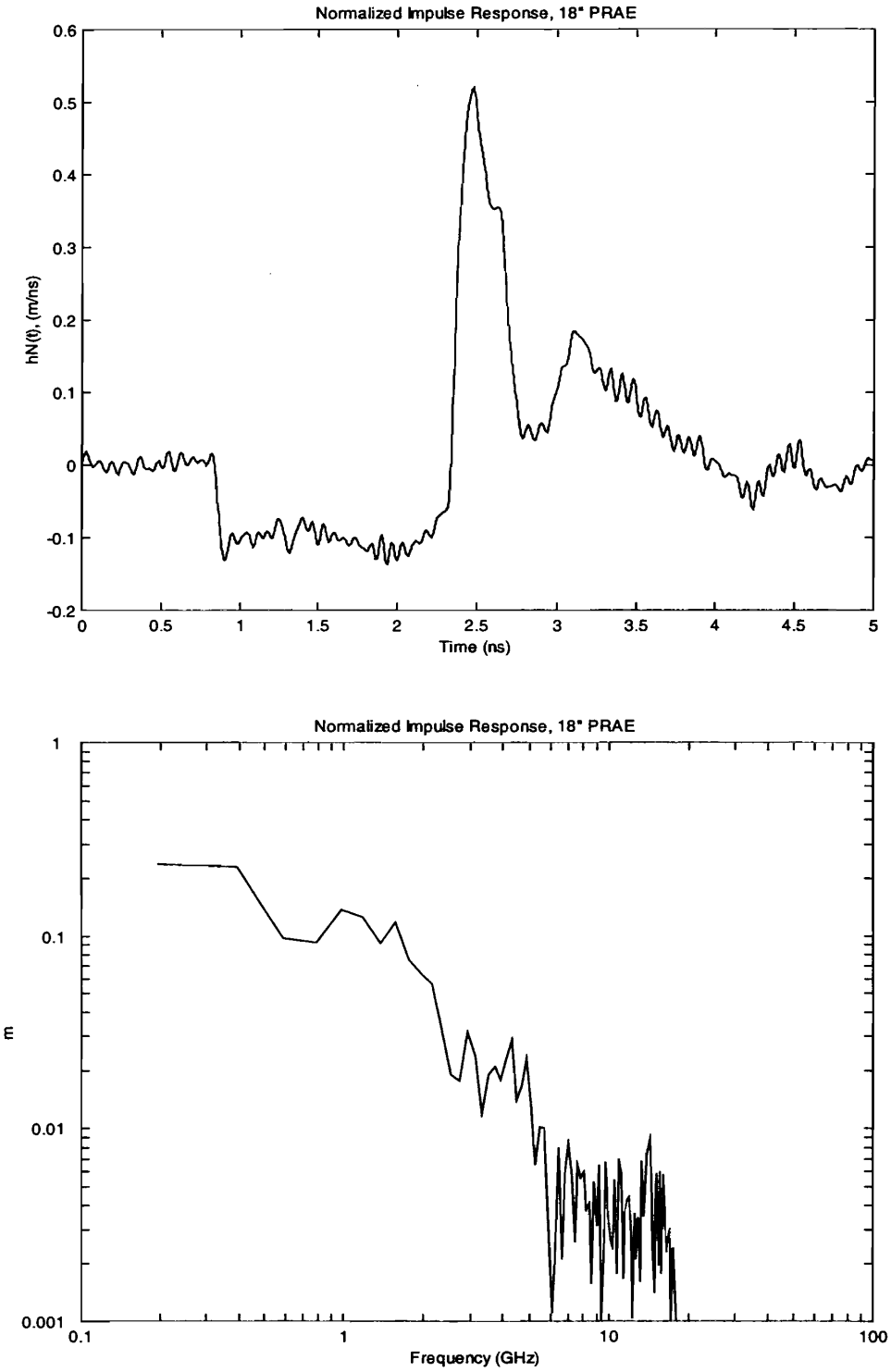

Figure 3.12. Impulse response of the PRAE, in the time domain (top) and in the frequency domain (bottom).

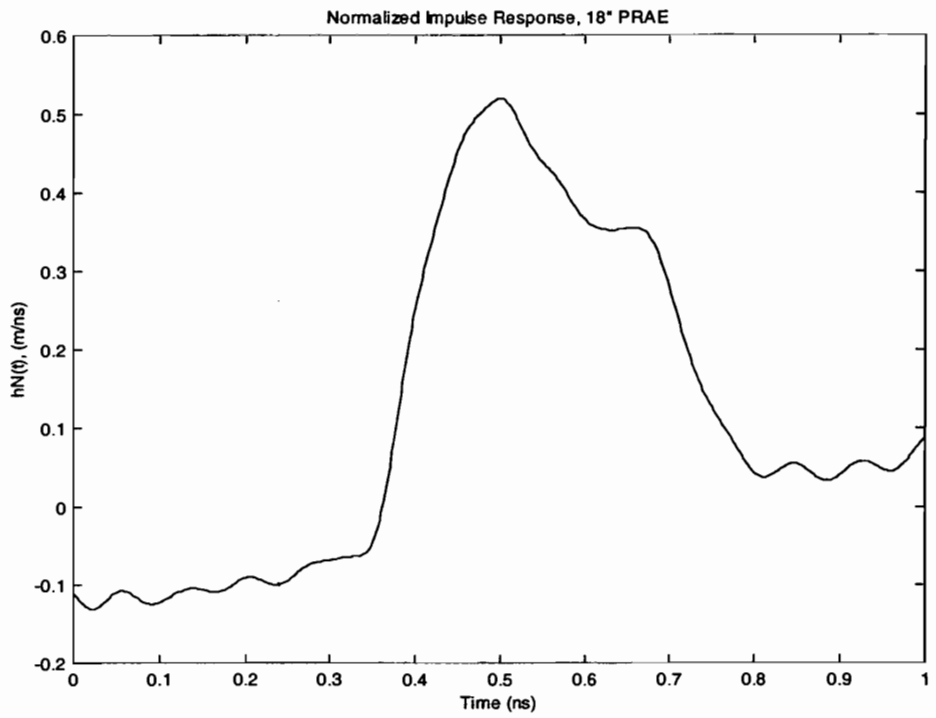

Figure 3.13. Close-up of the impulse response of the PRAE.

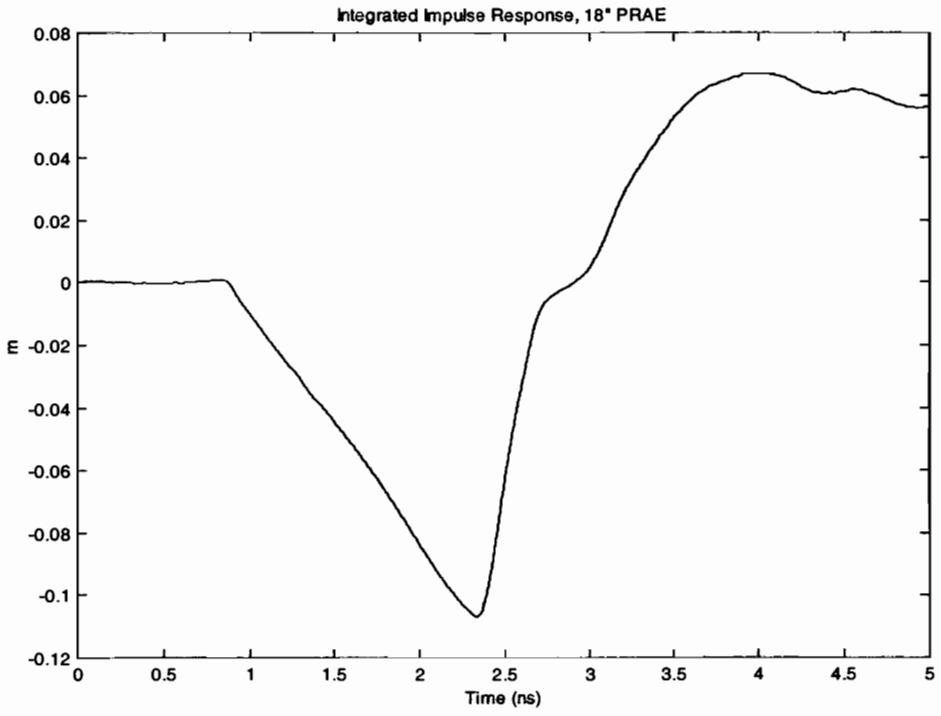

Figure 3.14. Integral of the impulse response of the PRAE.

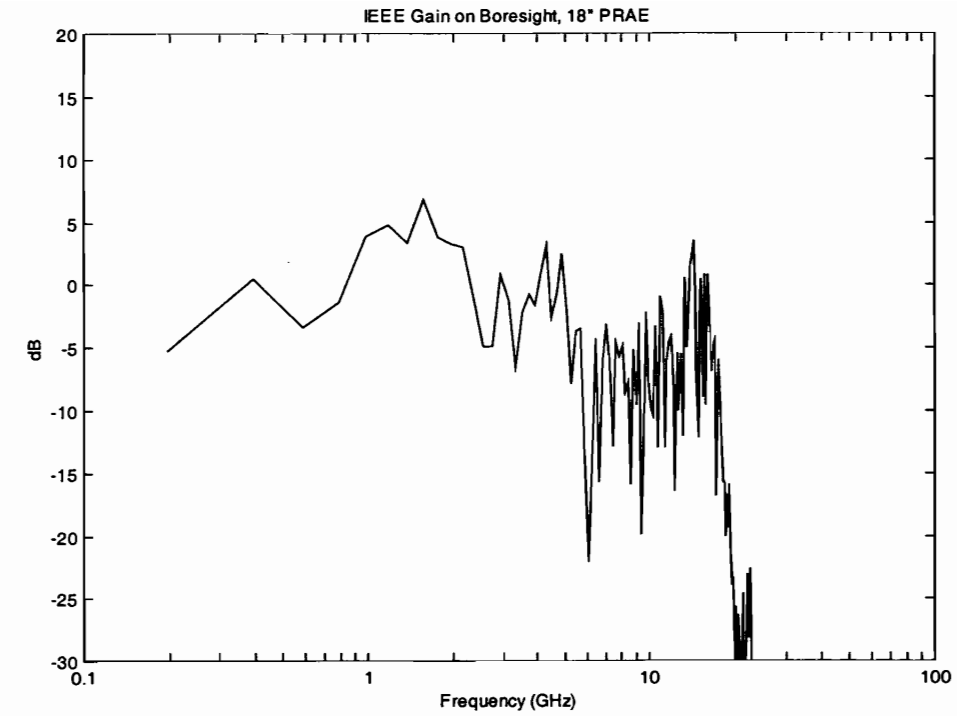

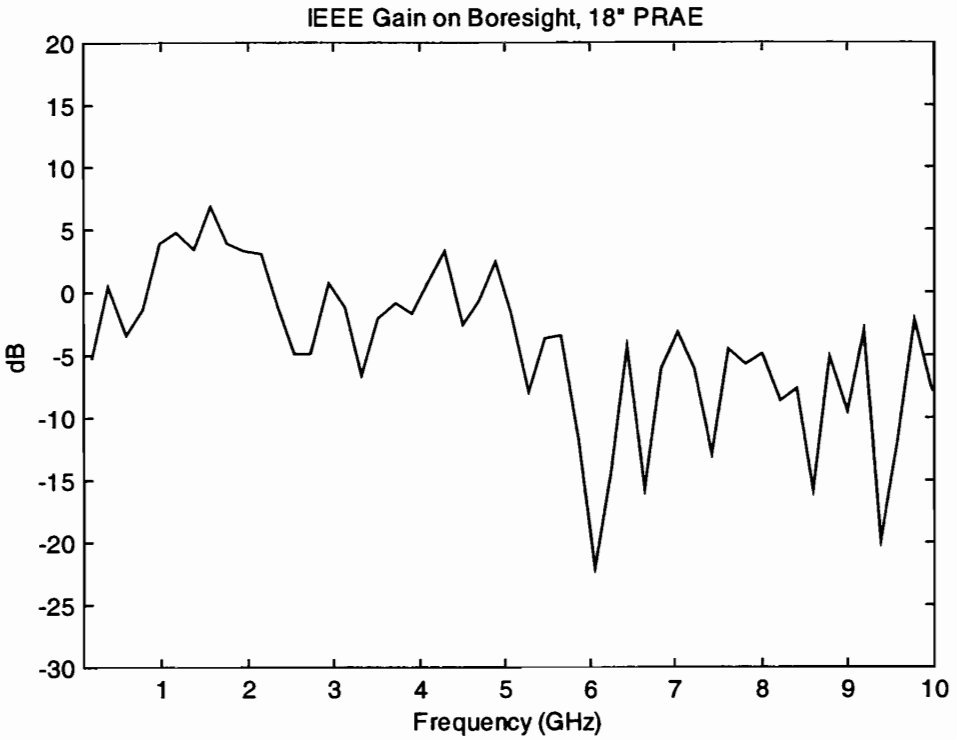

Figure 3.15. Gain of the PRAE on boresight, plotted on two different scales.

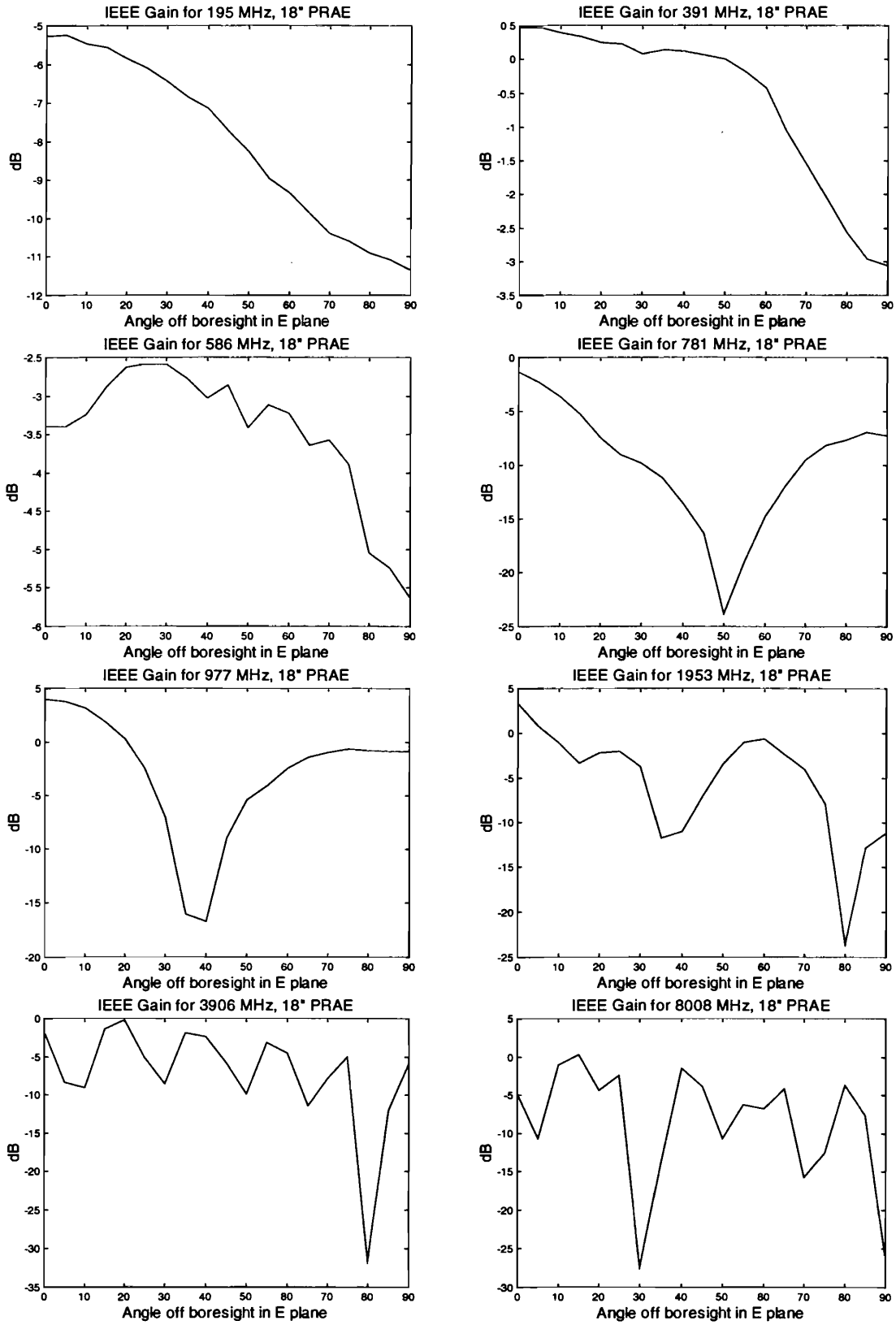

Figure 3.16. Gain of the PRAE as a function of angle in the E-plane, at 195, 391, 586, 781, 977, 1953, 3906, and 8008 MHz.

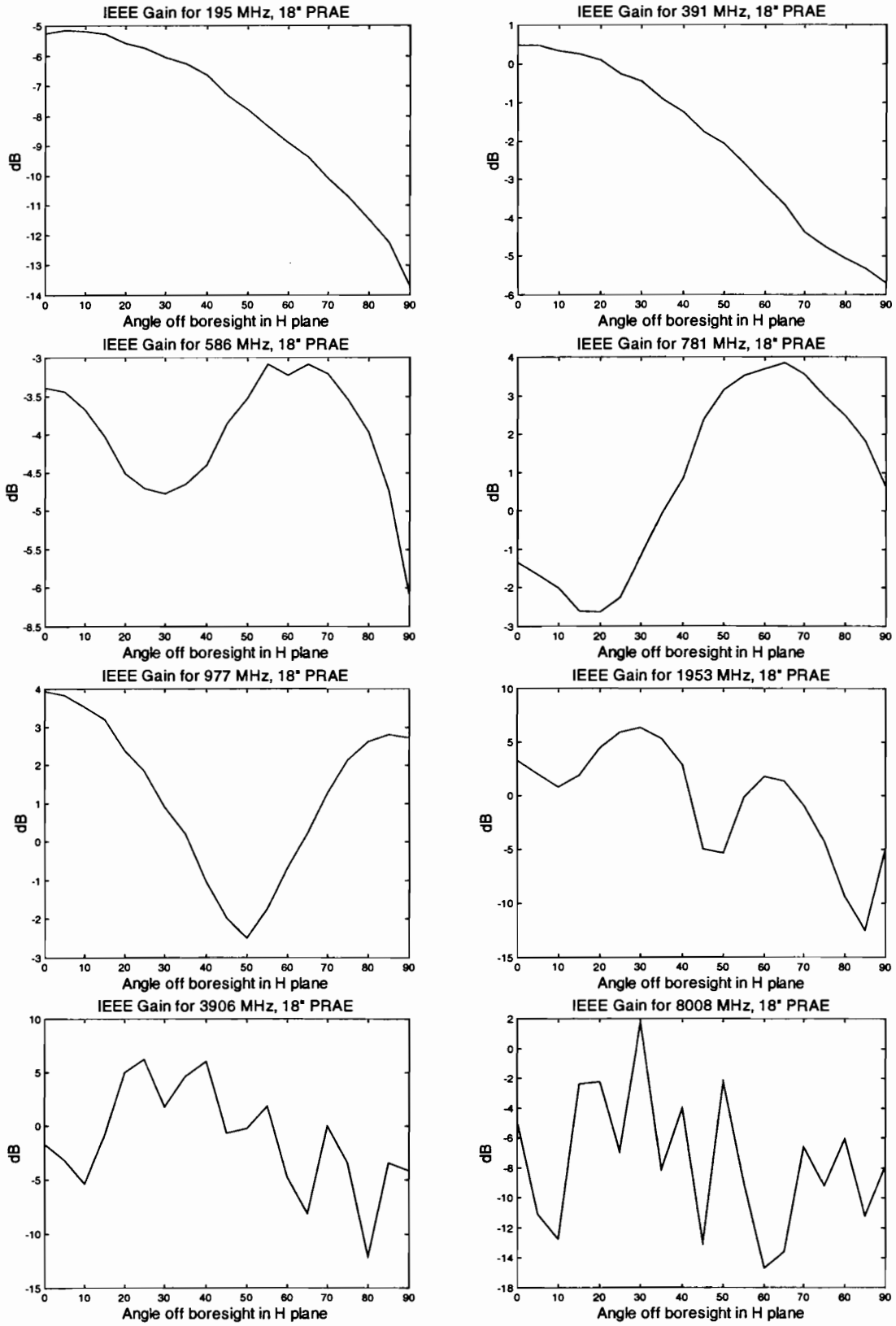

Figure 3.17. Gain of the PRAE as a function of angle in the H-plane, at 195, 391, 586, 781, 977, 1953, 3906, and 8008 MHz.

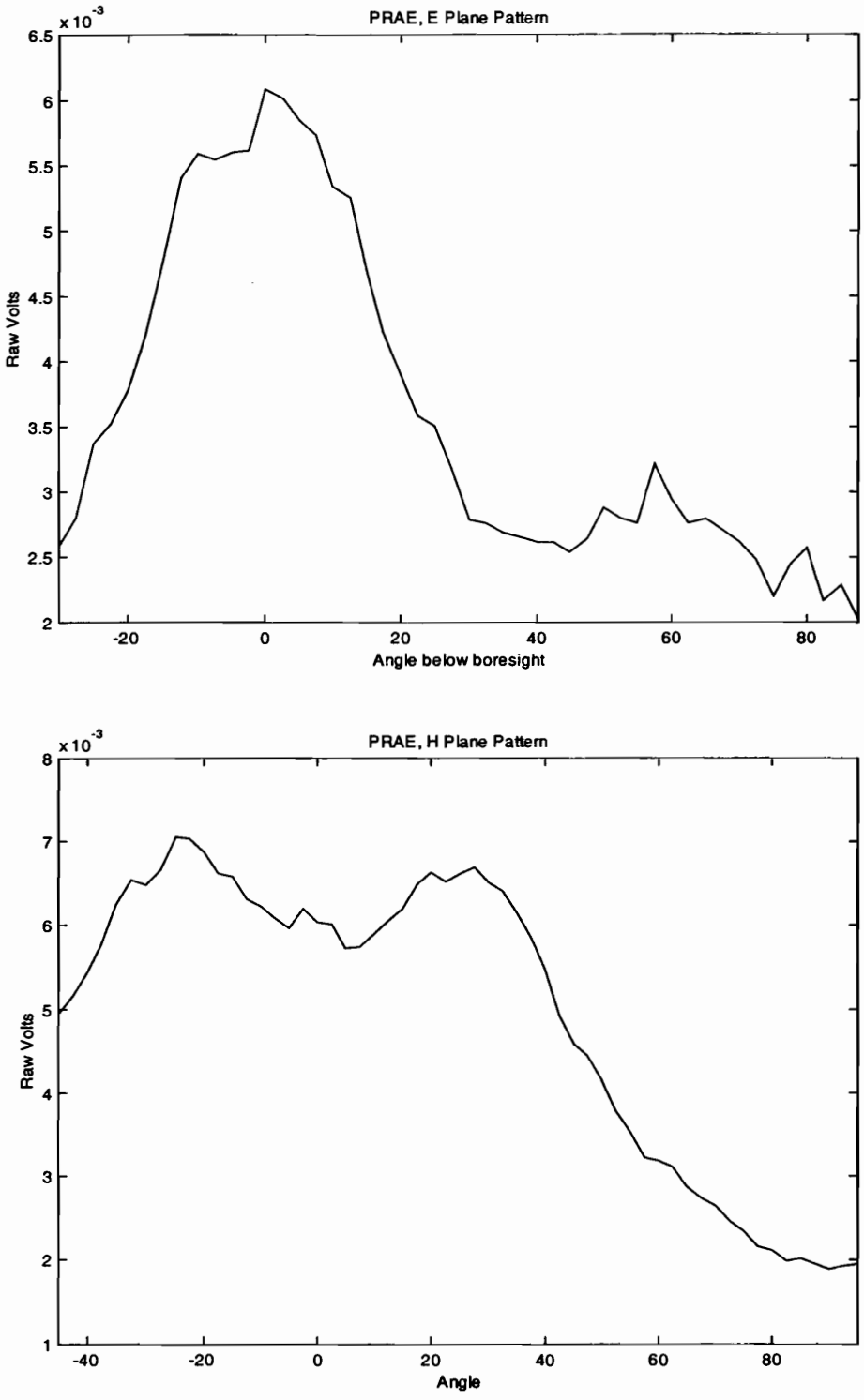

Figure 3.18. Antenna pattern of the PRAE in terms of peak raw voltage in the E-plane (top) and the H-plane (bottom).

IV. Frequency Domain Measurements

A. Introduction

Frequency domain measurements of the IRA and PRAE antennas were performed in Mission Research Corporation's compact antenna range. The facility, located in Dayton, Ohio, uses a focus fed compact range reflector and a broad band, coherent, pulsed, stepped-CW radar. As many as four channels, three frequencies, and two polarizations may be simultaneously recorded during a single antenna pattern measurement. The system offers a high degree of accuracy, speed, and interactive diagnostic capability in each of four domains:

- Fixed Frequency Angular Pattern.
- 0.2 - 18 GHz coherent spectrum at a fixed look angle.
- High resolution (0.0625 ns) Fourier transformed impulse response at a fixed angle.
- Wide band imaging.

MRC's compact range utilizes a $16' \times 15'$ rolled edge reflector to collimate a plane wave. The specifications for the compact range are given in Table 4.1. A picture of the anechoic chamber with the IRA antenna is shown in Figure 4.1.

Table 4.1. MRC Compact Range Specifications

Chamber Dimensions	$60' \times 24' \times 23'$
Frequency Coverage	0.2 - 2.2 GHz and 2.0 - 18 GHz
Quiet-Zone Size	$8' \times 6'$
Sensitivity	-75 dBsm
Dynamic Range	100 dB
Amplitude Ripple	0.2 dB (peak) (2-18 GHz band)
Amplitude Taper	$<$ ~1.0 dB (2-18 GHz band)
Cross Polarization Level	$<$ -25 dB

B. Measurement Configuration

Full polarimetric measurements of the IRA and PRAE antennas were performed in the MRC chamber. These calibrated measurements included principal plane patterns (E and H planes) as well as planar cuts rotated every 5° about boresight. Frequency sweeps from 200 MHz to 10 GHz were broken into two bands covering the frequency bands of 200 MHz to 2 GHz and 2 GHz to 10 GHz. High band measurements were made with the compact range reflector whereas direct illumination measurements were made for the low band. Far field requirements were satisfied in both cases.

Principal plane cuts were measured every 10 MHz and 2° throughout the entire plane (360°). Great circle cuts were made every 20 MHz and 2° throughout the forward half space (180°). Both horizontal and vertical polarization measurements were performed for the complete frequency/angle test matrix.

The results for the IRA and PRAE antennas are shown in the following sections. The metrics used in the following sections to characterize the performance of the IRA and PRAE antennas are described in detail in references [5]-[9].

C. IRA Measurements

The frequency domain results for the IRA antenna are presented in this section. The following results show that the IRA antenna is an extremely good broadband radiator that includes the following desirable features.

- The phase response is a linear function of frequency on boresight.
- The beamwidth is similar to that of an aperture antenna.

Figure 4.1. The IRA antenna under going tests in MRC's anechoic chamber.

- The radiated field is non-dispersive in the time domain.
- The boresight response is well behaved in both amplitude and phase.

However, the thorough characterization of the IRA antenna also identified several areas that need improvement. Most notable were the following:

- The large cross-polarization terms, particularly above 4 GHz need improvement.
- Evidence of multiple radiation mechanisms is present.
- High side lobe levels.
- A ring down in the antenna is observed around 4 to 6 ns near boresight.
- Dispersion off boresight.

Because the cause of most of these unwanted characteristics appear to be due to construction technique, it is expected that these unwanted features can be mitigated with further development of the antenna.

The following discussion highlights the characteristics identified during the frequency domain testing.

Boresight Response

The boresight response is shown in Figure 4.2. Significant features of the boresight response are:

- Co-polarized gain response agrees with time domain measurements shown in Figure 3.6.
- Cross-polarization isolation is greater than 20 dB below 2 GHz (measurement is noise limited below 1.5 GHz).
- Cross-polarization isolation is down to 10 dB by 4 GHz and deteriorates to 0 dB by 8 GHz.
- Boresight response (amplitude and phase) is well behaved.

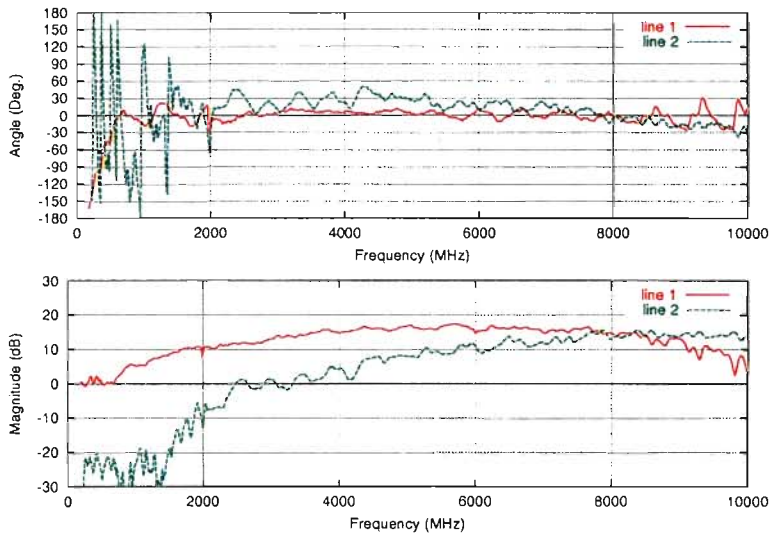

Figure 4.2. Boresight magnitude response of the IRA. Although the boresight response is shown to 10 GHz, the following parameters use only the data from 200 MHz to 8 GHz – the effective radiation band of the antenna.

Normalized Spectral Pattern Functions

The normalized spectral pattern functions, shown in Figures 4.3 and 4.4, have the following features:

- Multiple radiation mechanisms are present and result in high side lobe levels.
- The 3 dB beamwidth is approximately 27° at 2 GHz and 10° at 6 GHz in the E-plane and 18° at 2 GHz and 6° at 6 GHz in the H-plane.

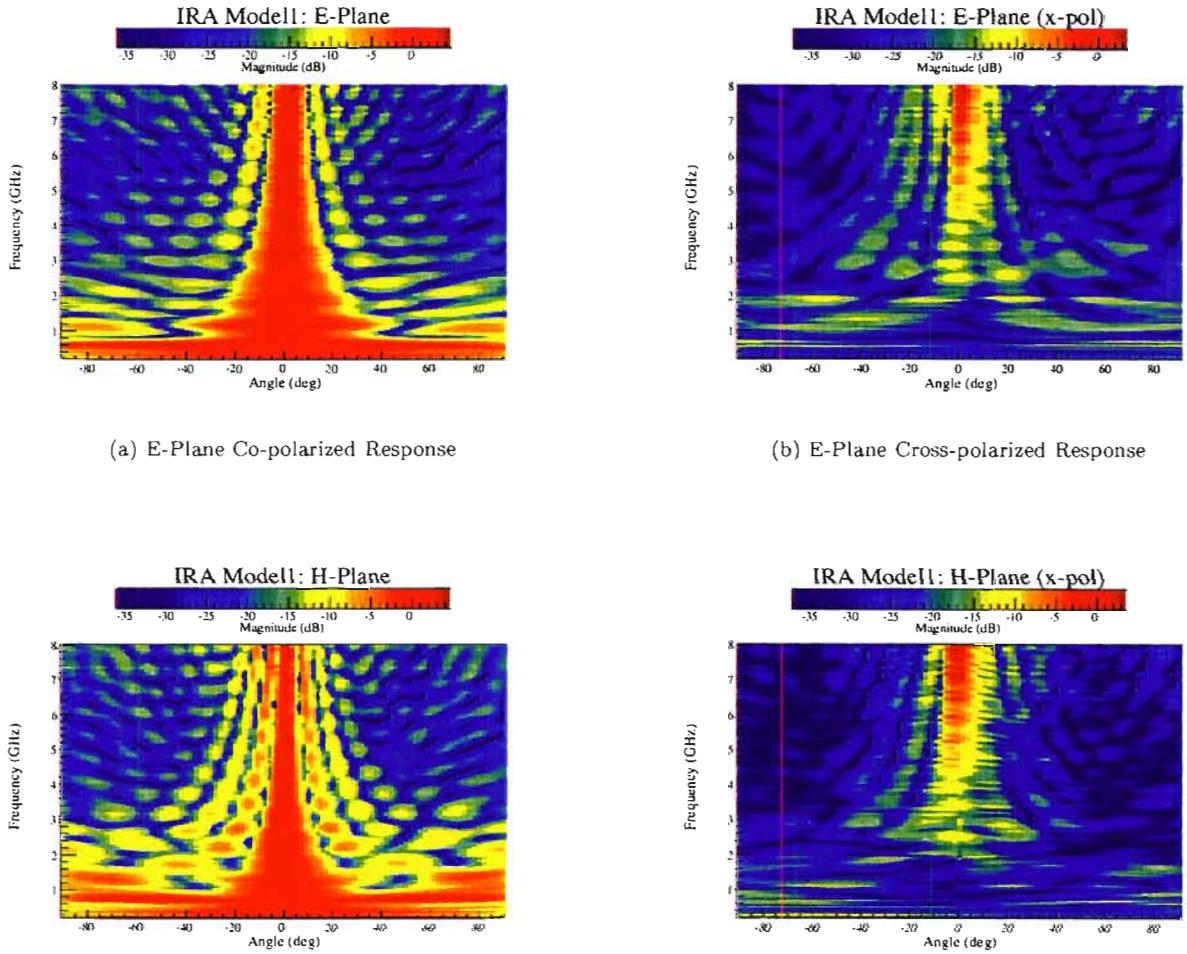

(a) E-Plane Co-polarized Response

(b) E-Plane Cross-polarized Response

(c) H-Plane Co-polarized Response

(d) H-Plane Cross-Polarized Response

Figure 4.3. The normalized magnitude spectral pattern functions for the principal planes of the IRA antenna.

Normalized Transient Pattern Functions

The normalized transient pattern functions are shown in Figure 4.5. These plots show the following characteristics:

- Multiple radiation mechanisms are visible as arc segments with different radiation centers.
- The phase center of higher order radiation mechanisms differ.

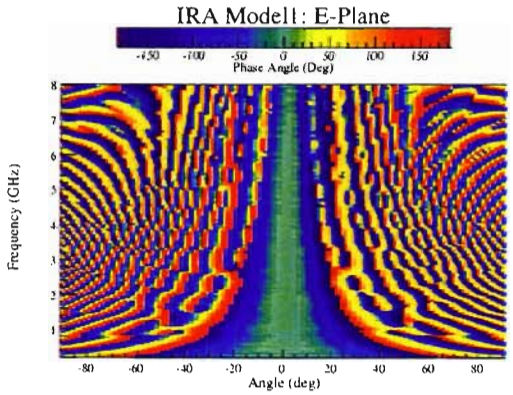

(a) E-Plane Co-polarized Response

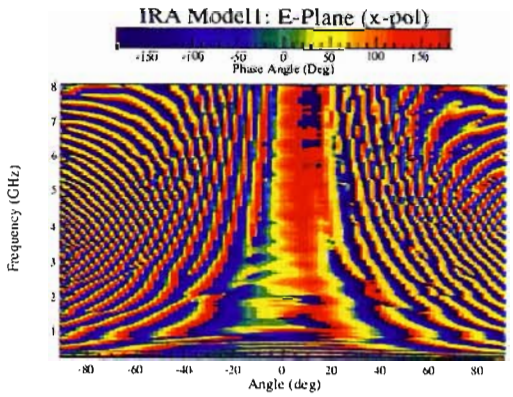

(b) E-Plane Cross-polarized Response

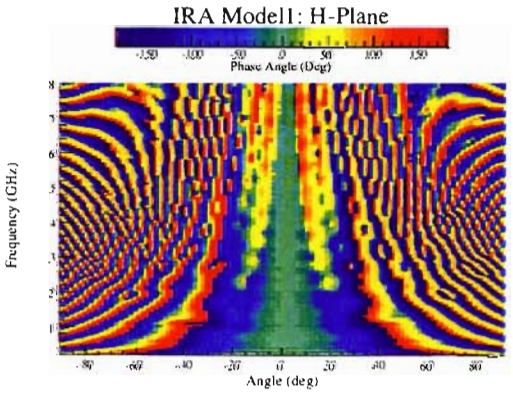

(c) H-Plane Co-polarized Response

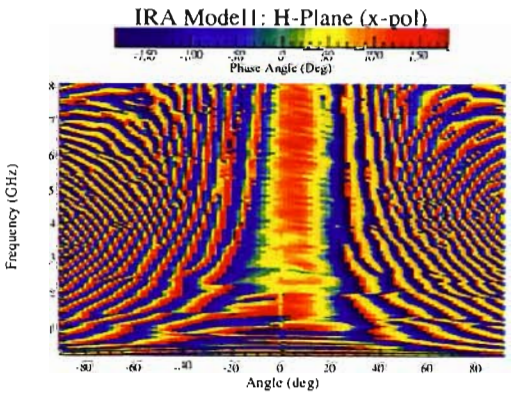

(d) H-Plane Cross-Polarized Response

Figure 4.4. The normalized phase spectral pattern functions for the principal planes of the IRA antenna.

- Antenna ring down, observed near 4 and 6 ns on boresight, is more significant in the cross polariation term.
- The pre-pulse is evident at early times.
- The pre-pulse has a different phase center than the primary reflection from the parabolic dish.

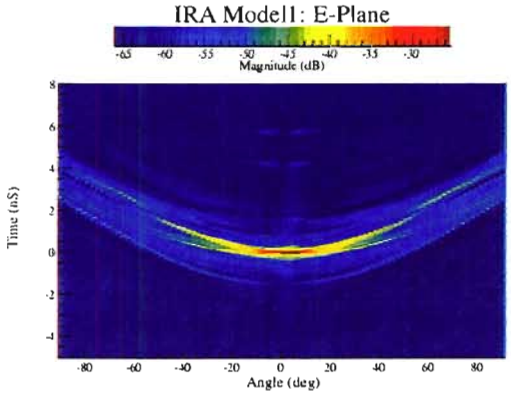

(a) E-Plane Co-polarized Response

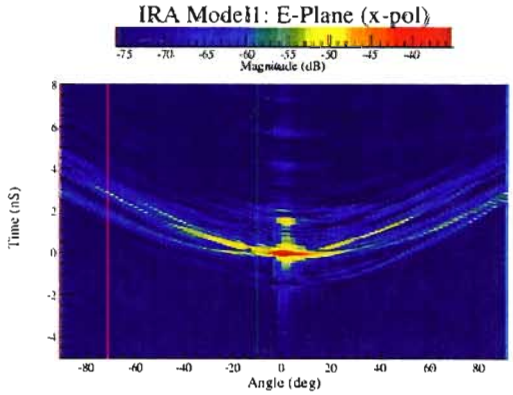

(b) E-Plane Cross-polarized Response

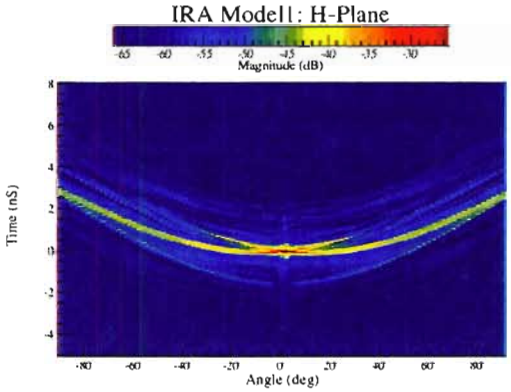

(c) H-Plane Co-polarized Response

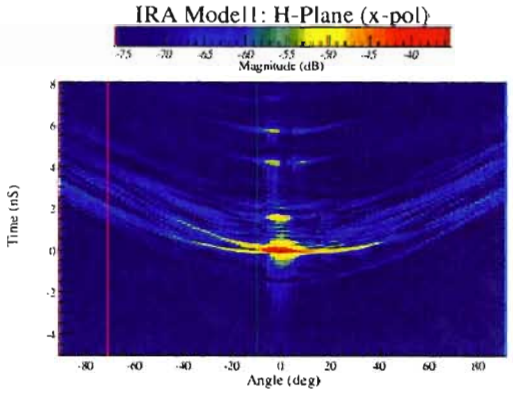

(d) H-Plane Cross-Polarized Response

Figure 4.5. The normalized transient pattern functions for the principal planes of the IRA antenna.

Normalized Energy Pattern Functions

The normalized energy pattern functions are shown in Figure 4.6. The following characteristics are observed:

- The overlaying of the peak and total energy curves near boresight indicate a low dispersion antenna response.
- Dispersion is evident off boresight as a separation between the peak and total energy curves.
- The E-plane beamwidth is greater than the H-plane beamwidth.

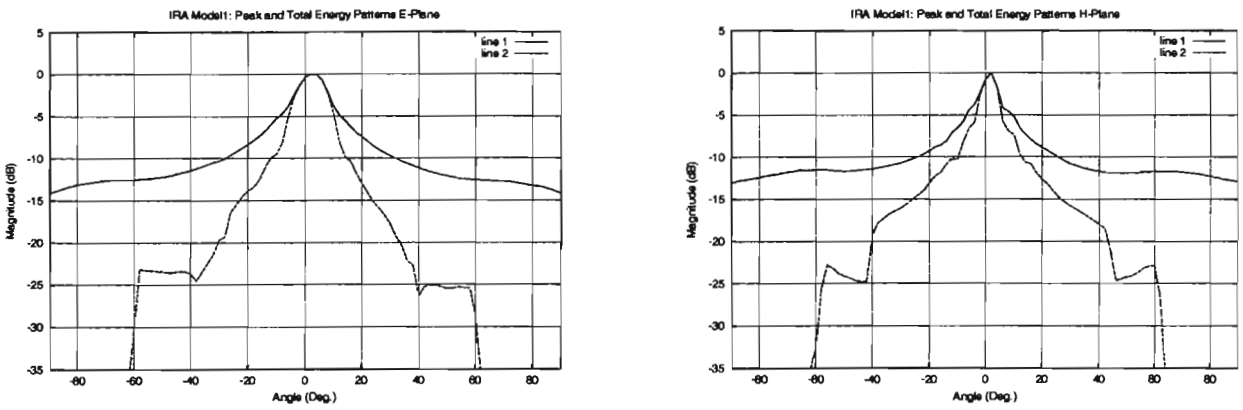

(a) E-Plane

(b) H-Plane

Figure 4.6. Peak and total energy pattern functions for the principal planes of the IRA antenna.

Energy Magnitude and Polarization Pattern Functions

The magnitude and polarization pattern functions are shown in Figure 4.7. The conclusions from these results are:

- The overall shape of the beam is well formed.
- The overall polarization isolation is poor when the entire operational bandwidth is considered (200 MHz to 8 GHz).

Ideal Point Target Images

The following images simulate a SAR image collection. The antenna is pointed 45° down from the horizon and oriented perpendicular to the line of flight. A 20° integration aperture that incorporates the full polarimetric behavior of the antenna was used to generate SAR images of ideal point targets located at different depression angles. A point target at a depression angle of 45° will travel through the boresight of the antenna with this SAR geometry and will, in general, produce the best image. Since free space losses have been removed, these images show variations due solely to the non uniform behavior of the antenna in frequency, angle, and polarization. The ideal point target images for the IRA antenna are shown in Figures 4.8 and 4.9 and should be compared to the reference image shown in Figure 4.10. The following characteristics are observed:

- The formed images are highly dependent on boresight normalization and aspect angle because of the higher order radiation mechanisms already identified.
- The E-plane response at 45° (boresight) closely resembles the reference image, but quickly deviates.
- Image quality is highly dependent on the direction chosen for boresight normalization and the SAR integration angle.

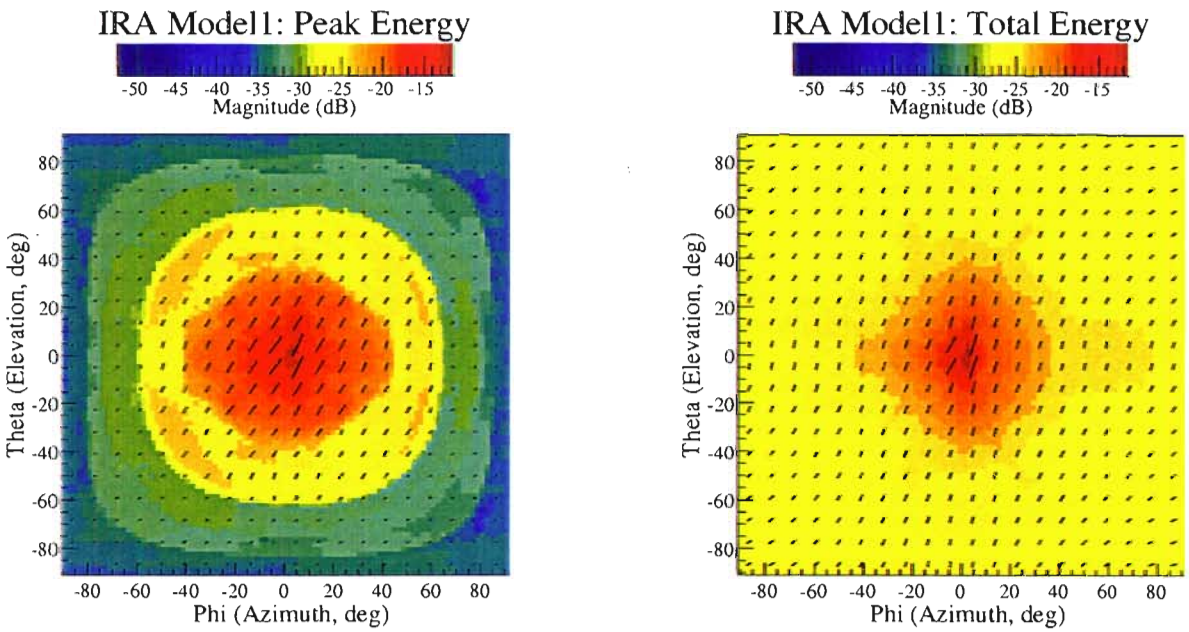

(a) Peak Energy Response

(b) Total Energy Response

Figure 4.7. Peak and total energy magnitude and polarization pattern functions of the IRA antenna.

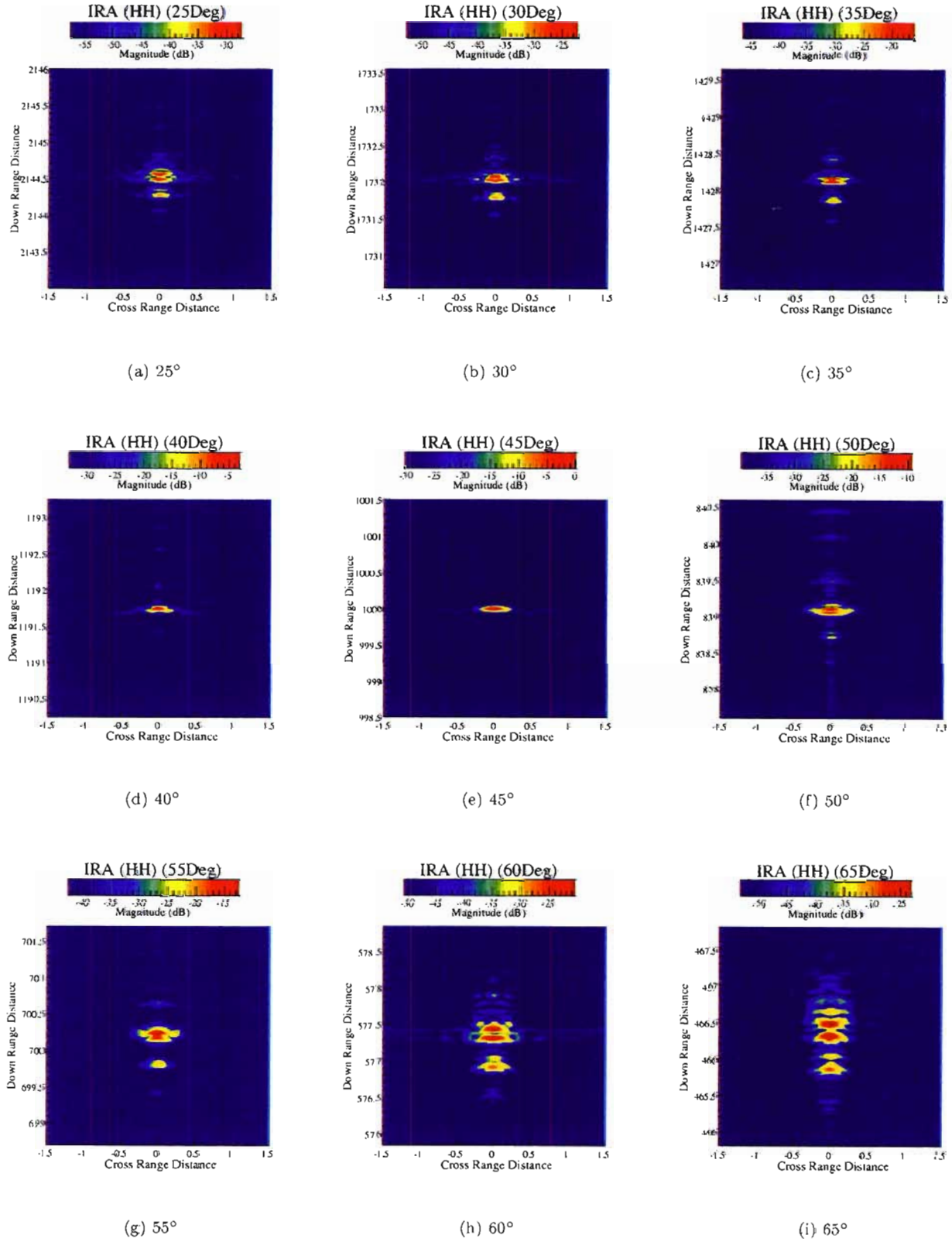

(a) 25°

(b) 30°

(c) 35°

(d) 40°

(e) 45°

(f) 50°

(g) 55°

(h) 60°

(i) 65°

Figure 4.8. Ideal point target image response at different depression angles for a horizontally polarized IRA antenna aligned with a depression angle of 45°.

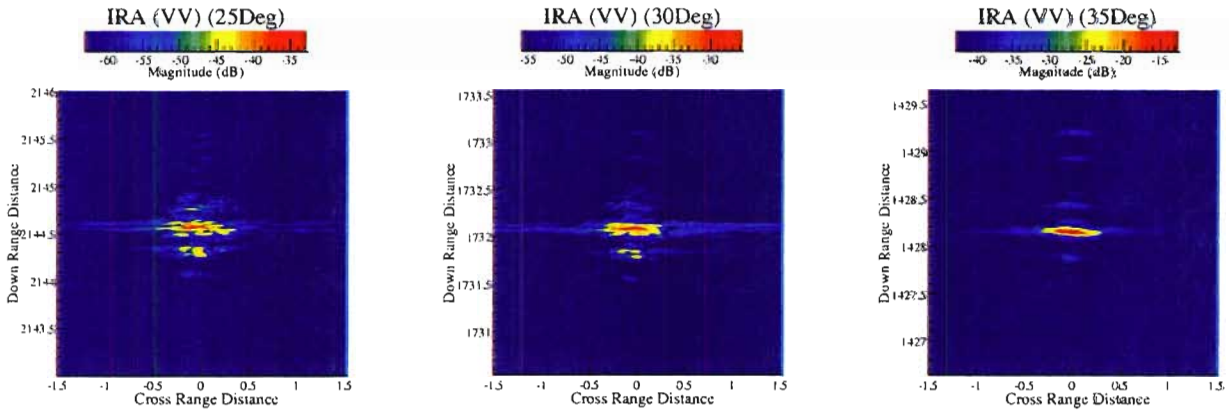

(a) 25°

(b) 30°

(c) 35°

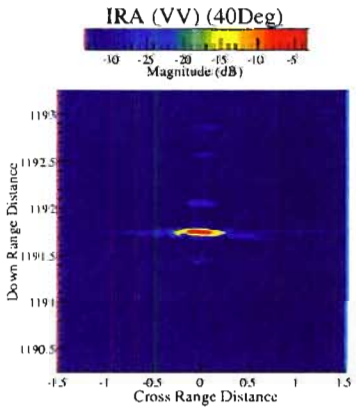

(d) 40°

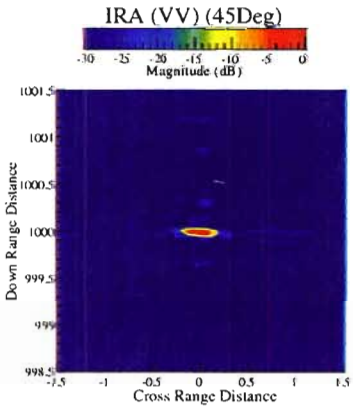

(e) 45°

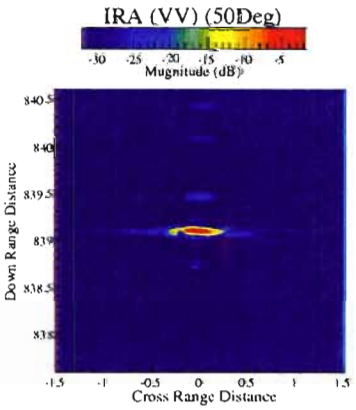

(f) 50°

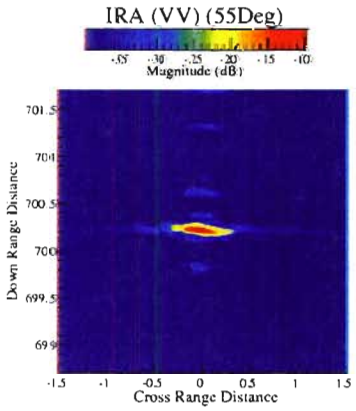

(g) 55°

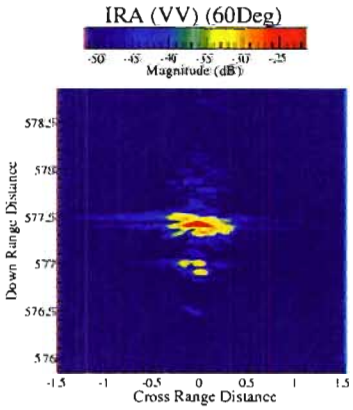

(h) 60°

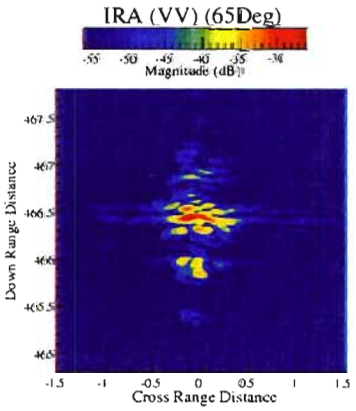

(i) 65°

Figure 4.9. Ideal point target image response at different depression angles for a vertically polarized IRA antenna aligned with a depression angle of 45°.

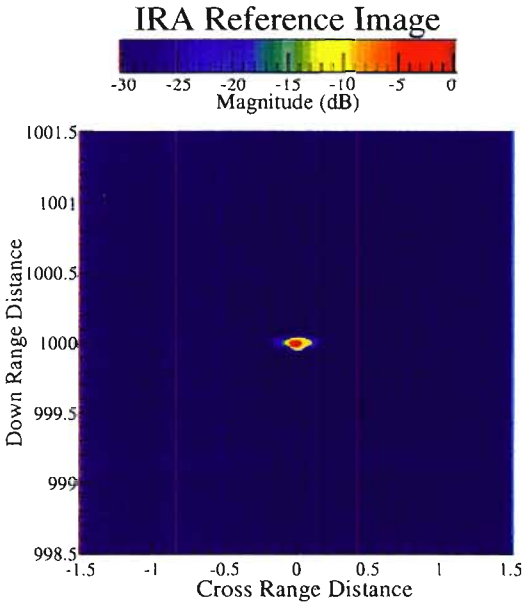

Figure 4.10. The ideal point target image response with an isotropic antenna response with imaging parameters identical to those for the IRA antenna.

D. PRAE Measurements

The frequency domain results for the PRAE antenna are presented in this section. In general, the PRAE antenna did not perform as well as the IRA antenna. It's polarization purity, bandwidth, and beamforming capabilities were significantly inferior to the IRA antenna. The general characteristics of the PRAE antenna are highlighted below.

Boresight Response

The boresight response, shown in Figure 4.11, has the following characteristics:

- Polarization isolation is poor above 2.5 GHz.
- The gain is significantly lower than the IRA antenna.
- Phase and amplitude has significant ripple.

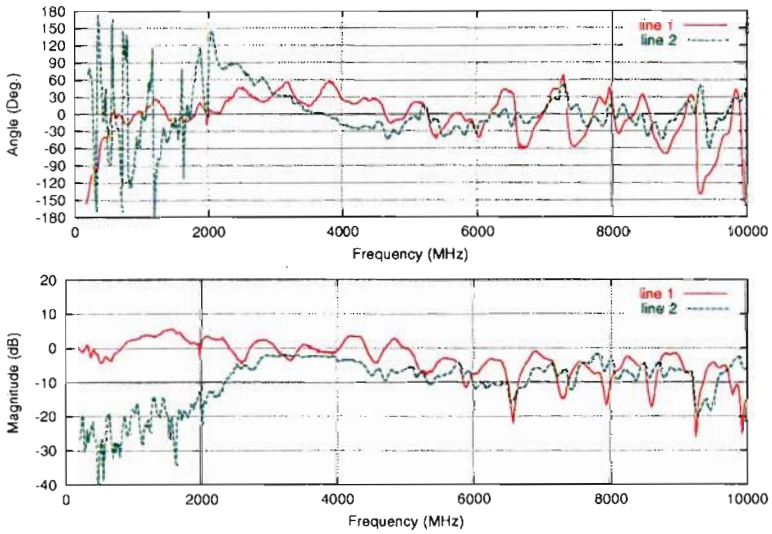

Figure 4.11. Boresight magnitude response of the PRAE. Although the boresight response is shown to 10 GHz, the following parameters use only the data from 200 MHz to 8 GHz.

Normalized Spectral Pattern Functions

The normalized spectral pattern functions, shown in Figures 4.12 and 4.13, illustrate the poor pattern performance of the PRAE antenna.

Normalized Transient Pattern Functions

The normalized transient pattern functions, shown in Figure 4.14, show the following features:

- Multiple radiation mechanisms are visible. Significant diffraction off of the reflector plates edges is seen 40° to 80° off boresight.
- The pre-pulse or direct radiation from the feed is nearly as strong as the reflected radiation which leads to the boresight gain ripple shown in Figure 4.11.
- Significant performance improvements may be possible if the ratio of the pre-pulse to reflected energy is reduced.
- Considering only the energy from the reflector, this antenna has nearly ideal pattern characteristics for a UWB SAR antenna (evident by the nearly constant response as a function of angle at time equal zero).

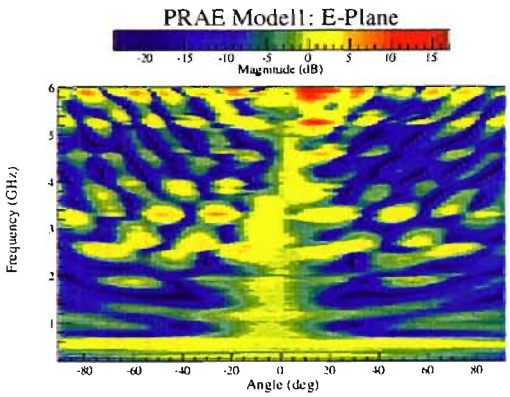

(a) E-Plane Co-polarized Response

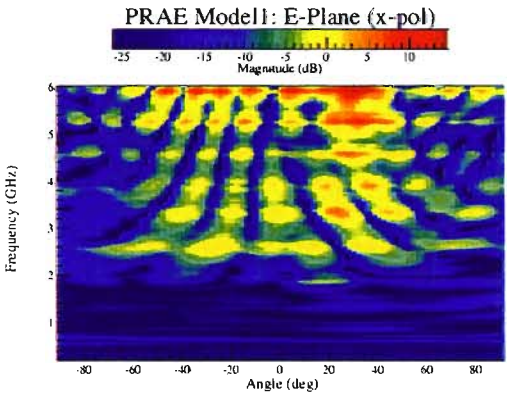

(b) E-Plane Cross-polarized Response

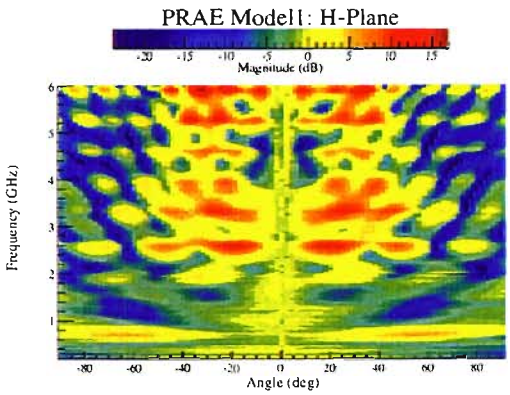

(c) H-Plane Co-polarized Response

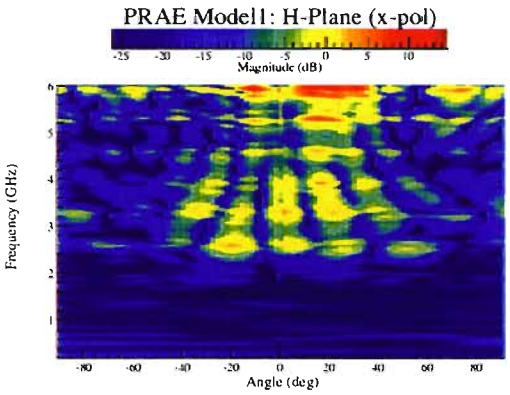

(d) H-Plane Cross-Polarized Response

Figure 4.12. The normalized magnitude spectral pattern functions of the PRAE antenna.

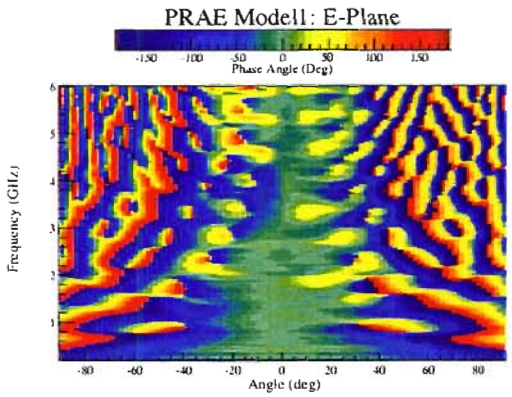

(a) E-Plane Co-polarized Response

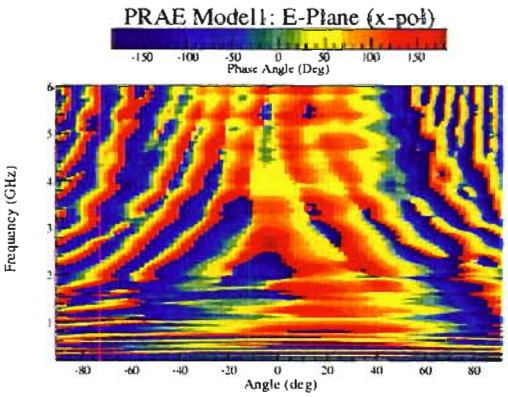

(b) E-Plane Cross-polarized Response

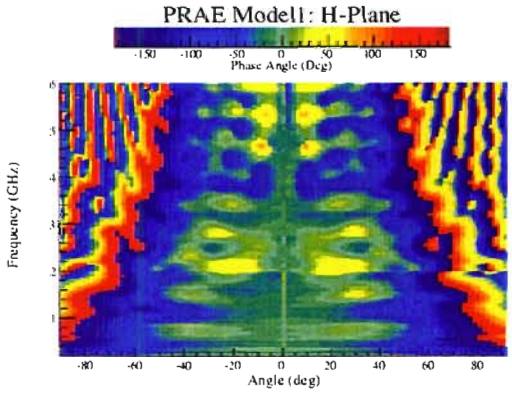

(c) H-Plane Co-polarized Response

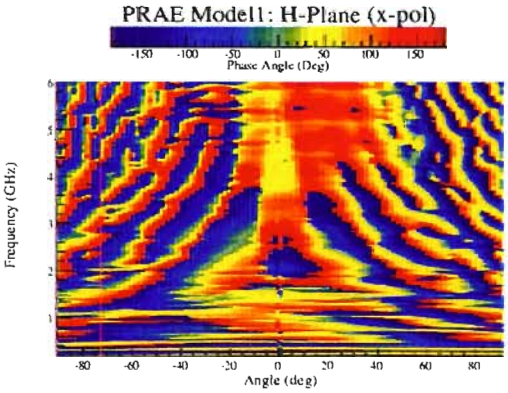

(d) H-Plane Cross-Polarized Response

Figure 4.13. The normalized phase spectral pattern functions of the PRAE antenna.

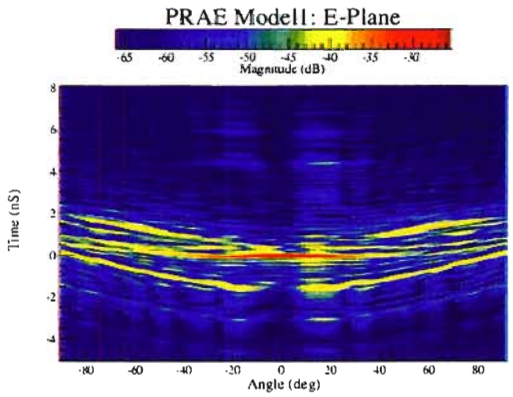

(a) E-Plane Co-polarized Response

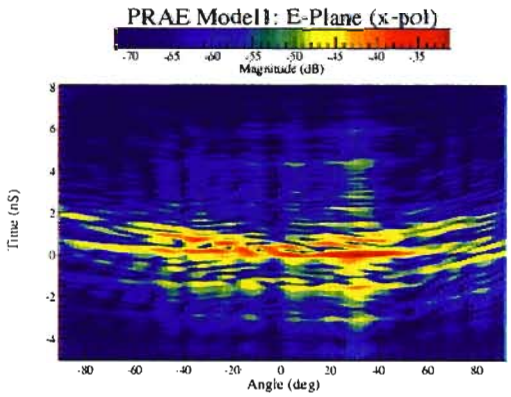

(b) E-Plane Cross-polarized Response

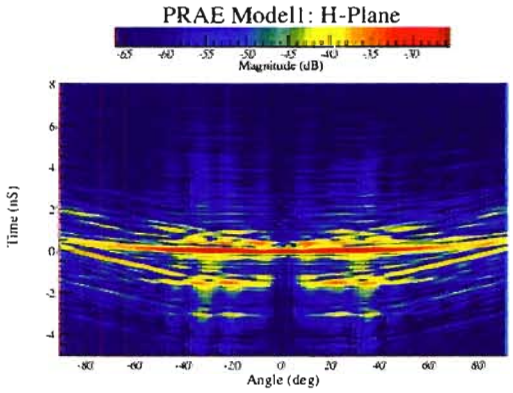

(c) H-Plane Co-polarized Response

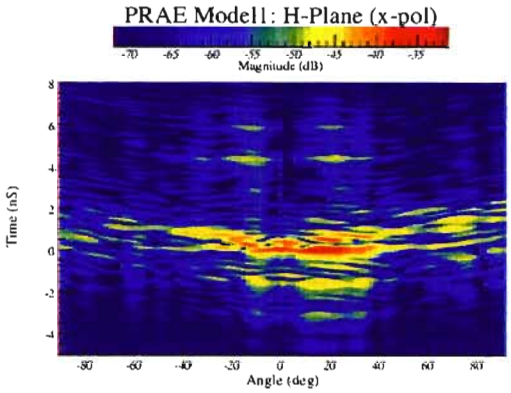

(d) H-Plane Cross-Polarized Response

Figure 4.14. The normalized transient pattern functions of the PRAE antenna.

Normalized Energy Pattern Functions

The normalized energy pattern functions are shown in Figure 4.15.

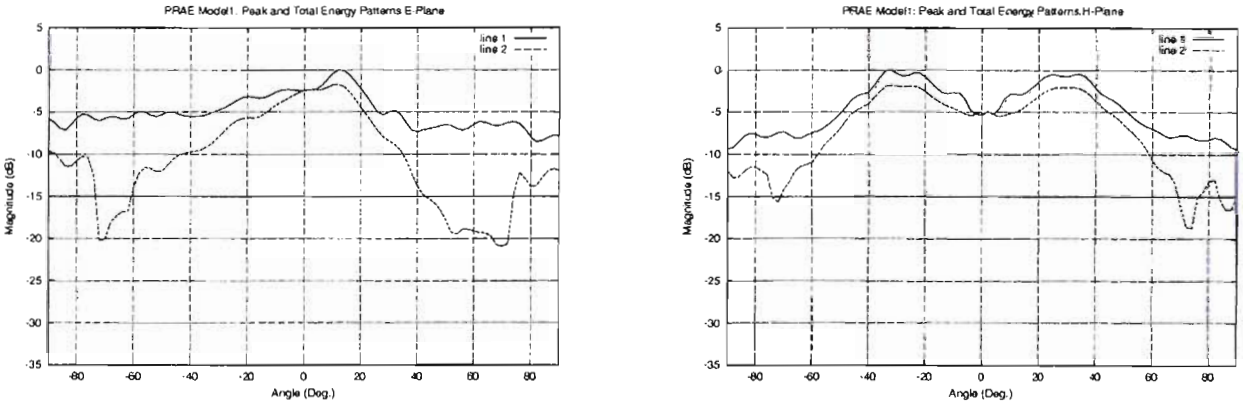

(a) E-Plane

(b) H-Plane

Figure 4.15. Peak and total energy pattern functions of the PRAE antenna.

Energy Magnitude and Polarization Pattern Functions

The magnitude and polarization pattern functions are shown in Figure 4.16.

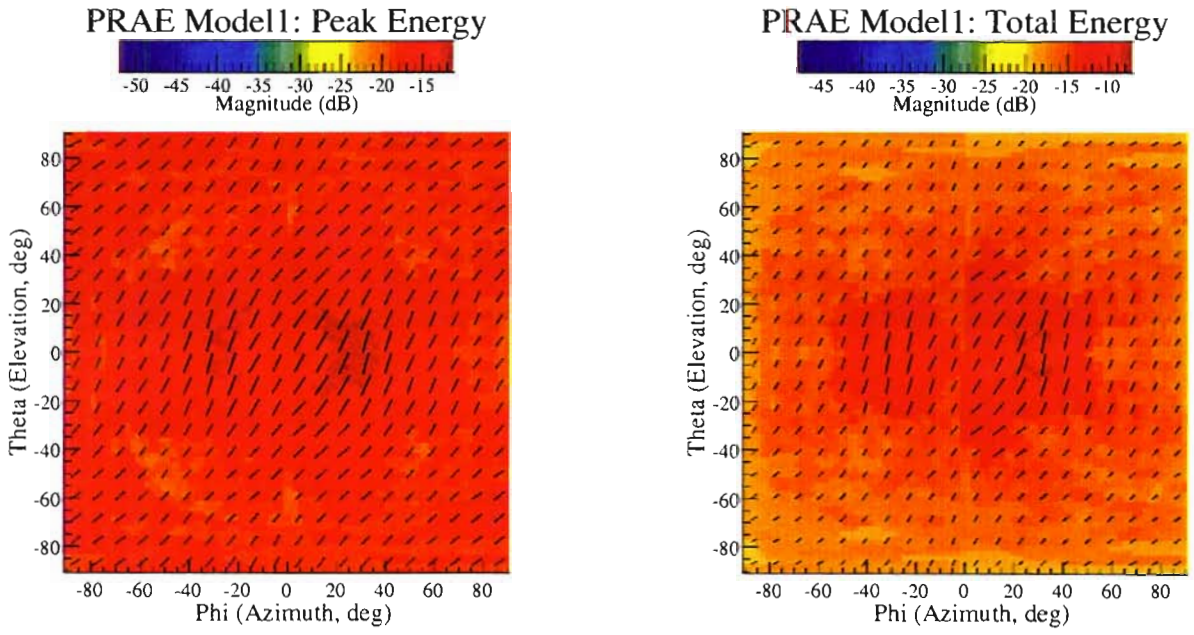

(a) Peak Energy Response

(b) Total Energy Response

Figure 4.16. Peak and total energy magnitude and polarization pattern functions of the PRAE antenna.

Ideal Point Target Images

The ideal point target images are shown in Figures 4.17 and 4.18. These images should be compared to the reference image shown in Figure 4.19 and have been generated in a manner identical to the IRA SAR images.

- In its current configuration, the PRAE antenna is not suitable as an UWB SAR antenna.

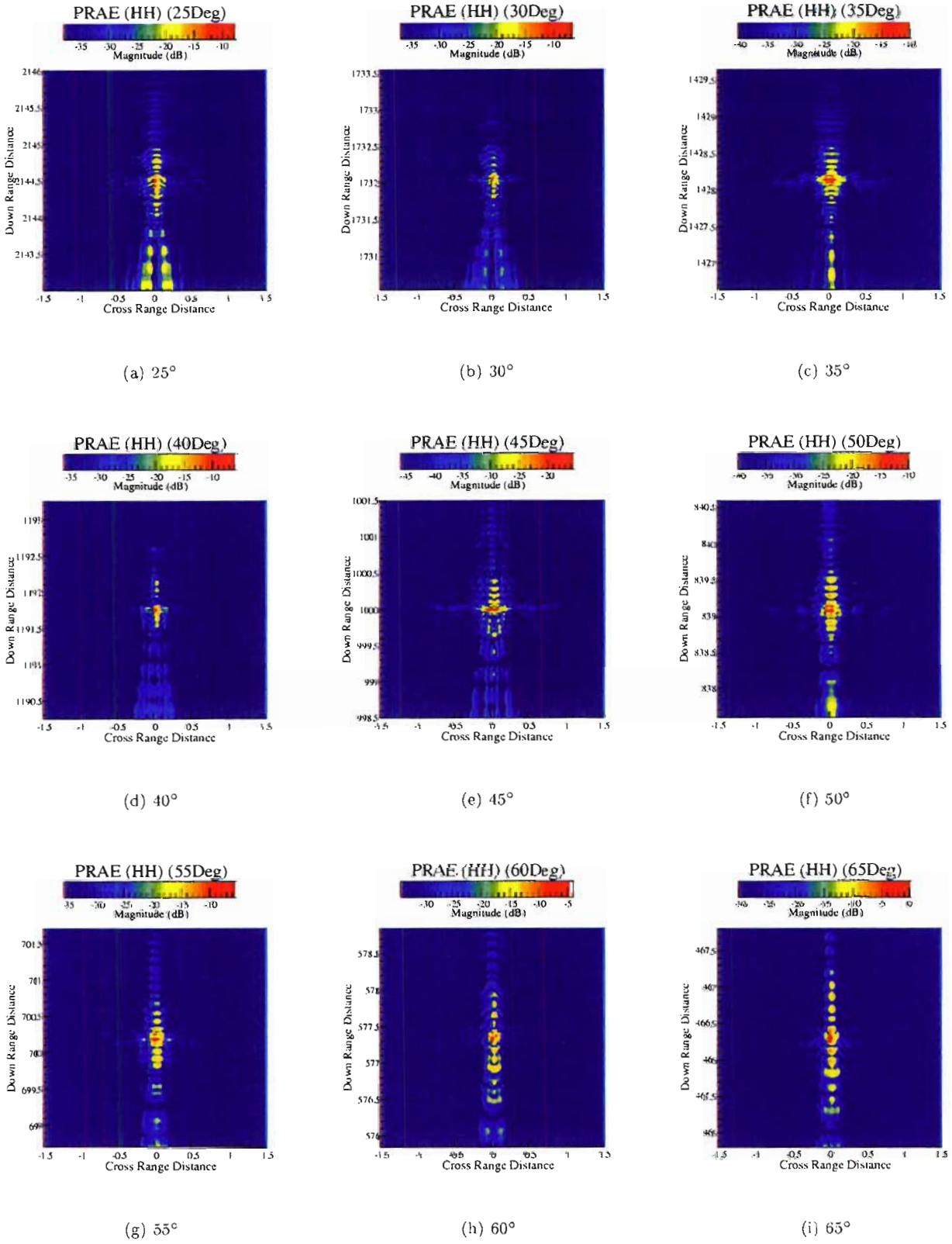

(a) 25° (b) 30° (c) 35°

(d) 40° (e) 45° (f) 50°

(g) 55° (h) 60° (i) 65°

Figure 4.17. Ideal point target image response at different depression angles for a horizontally polarized PRAE antenna aligned with a depression angle of 45°.

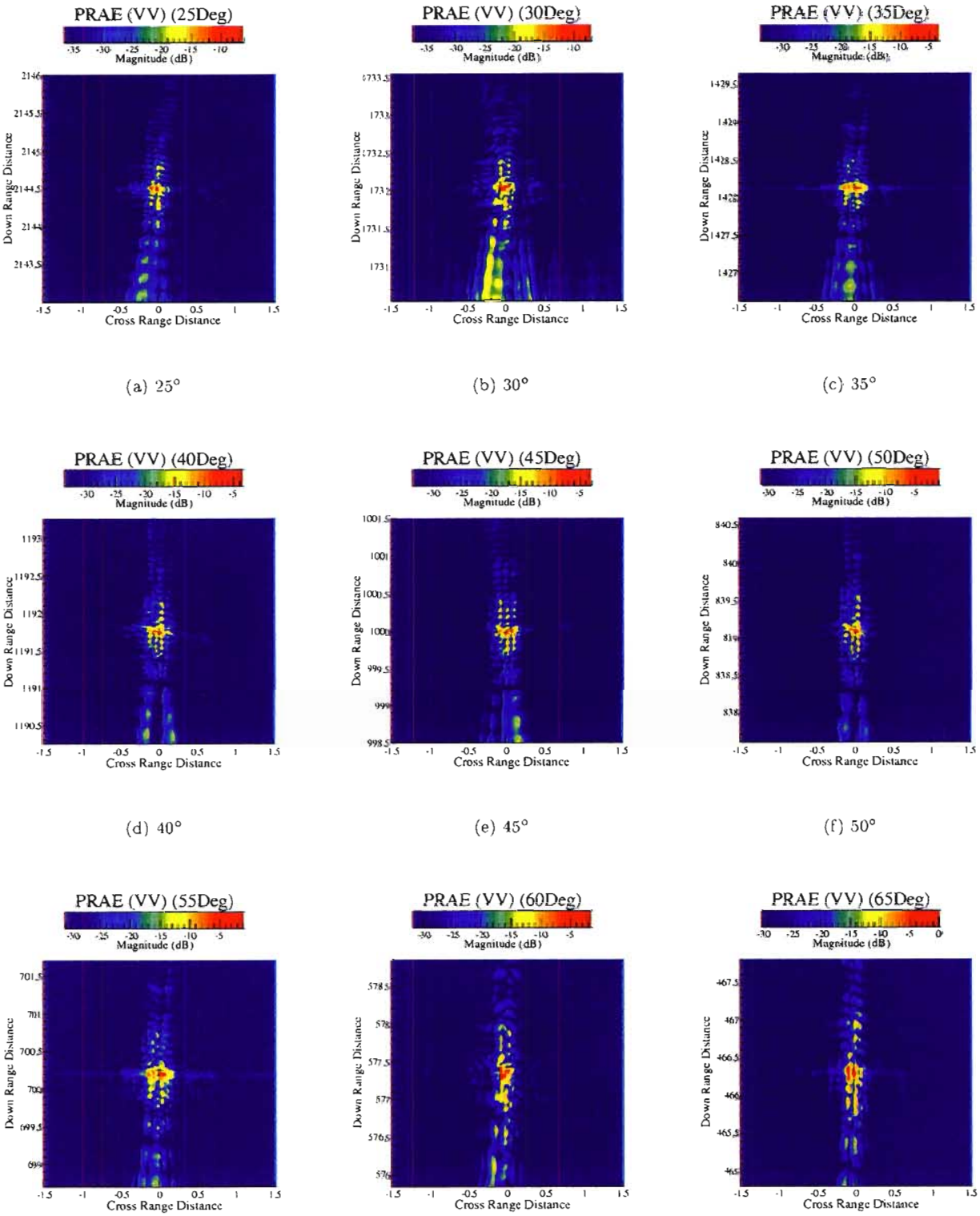

(a) 25°

(b) 30°

(c) 35°

(d) 40°

(e) 45°

(f) 50°

(g) 55°

(h) 60°

(i) 65°

Figure 4.18. Ideal point target image response at different depression angles for a vertically polarized PRAE antenna aligned with a depression angle of 45°.

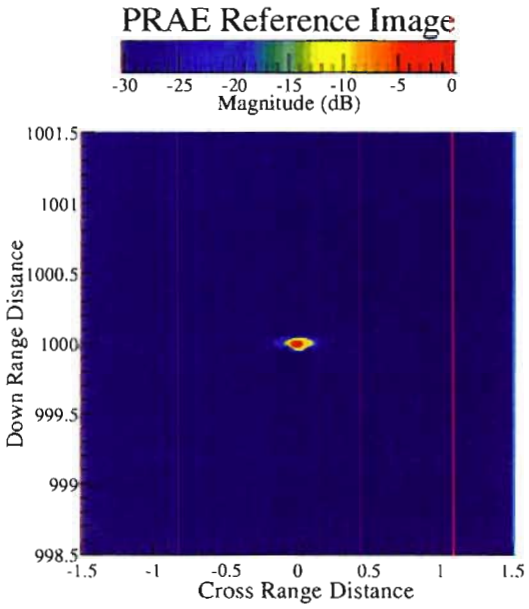

Figure 4.19. The ideal point target image response with an isotropic antenna response with imaging parameters identical to those for the PRAE antenna.

V. Comparison of the Time and Frequency Domain Data

It is of considerable interest to compare the frequency domain and time domain gain patterns. We do so in order to validate the measurements made on the Farr Research time domain range.

We begin with a comparison of the gain of the IRA on boresight, as a function of frequency. The data from the time domain is shown in Figure 3.6 and the data from the frequency domain is shown in Figure 4.2. In the time domain data, we see that the IRA has a peak gain of around 15 dB. Furthermore, there is a band of frequencies between 2 and 9 GHz in which the gain is above 10 dB. This compares well with the frequency domain data, where we see the same features.

The above comparison of frequency and time domain data demonstrates that the two techniques are essentially similar. Although we have not yet provided a detailed comparison, we can verify that a time domain range can be used to quickly check out broadband antenna designs.

Next, we consider the features that are more apparent in the frequency domain measurements than in the time domain. Consider the antenna patterns of the IRA as shown in Figure 4.3. Here we see that there are side-lobes 9 dB down from the main beam. The analogous patterns from the time domain data are in Figures 3.7 and 3.8. It appears in the time domain data that a lobed pattern is forming, but there is insufficient resolution to see the lobes clearly. If the time domain system were automated, the lobes might become more apparent, because data could be taken at smaller angular increments.

Finally, we note that because of the automation of the frequency domain system, a complete set of cross-pol data has been collected. While polarization data could easily be collected with the time domain system, the manual work would be double what it already is. This suggests that further automation in the time domain system would be very helpful.

VI. Application to SAR and Remote Target ID

We consider here new applications for the class of antenna we have built and tested. A key feature of these applications is that it is not necessary to radiate a clean impulse; we are merely taking advantage of the broad bandwidth of the antenna.

A. Synthetic Aperture Radar

Existing Foliage Penetration (FOPEN) SAR systems generally operate in the frequency range of 100 MHz to a few GHz. It has already been demonstrated that either TEM horns [10,11] or log periodic antennas [6] are capable of fulfilling this mission. However, there is a configuration of SAR that is generally referred to as "spotlight-mode", which may require a different antenna. With spotlight-mode, the beam is more narrow than with the more general case. Furthermore, the antenna rotates such that the beam is always pointed at the center of the SAR field on the ground. It is expected that spotlight mode will provide better focus than conventional SARs. The narrow pattern of the IRA, combined with its broad bandwidth, may prove to be quite useful for this mode.

One of the reasons we built the PRAE was that we thought an IRA with a broader pattern would be useful for conventional SAR, as a replacement for the TEM horn or log-periodic antennas. In fact, the PRAE provides a gain of approximately 0 dB up to a frequency of 5 GHz. This may be acceptable in some systems, however it is our impression that most SAR systems require a higher gain.

B. Target Identification

There is a group of investigators that has been investigating non-cooperative target identification. The most common method of identification is imaging, but they are considering other techniques as well, such as pole extraction. They have generally operated near X-band, but they would be able to take advantage of information at lower frequencies if it were available to them. The IRA seems to be an antenna that can provide this community with a broadband antenna that covers X band and lower, with a size and shape that is compatible with many system designs. Note that in this case a log-periodic antenna does not work, because they are generally not built to operate above a few gigahertz.

VII. Recommendations for Future Work

The existing design of the apex, using a splitter balun with connections for two cables, is delicate and easy to break. A new design is needed that is more robust, and this is currently being developed.

The apex with two feed cables limits the high-end bandwidth of the IRA. This is a result of deviations from perfect conical symmetry near the apex, because of the presence of cable. To address the bandwidth problem, one would consider splitting the antenna into two halves with a ground plane located in a plane of symmetry. Each half would then be fed by a single 100-ohm cable. This design will be addressed in a future project.

The side lobe level of 9 dB at in the (E or H)-plane plot is higher than we would like for many of these applications. It is standard practice to treat the edge of the reflector with either resistive card or a ragged edge to cut down on diffraction. There is no reason why this would not be helpful in broadband designs as well. We note that the side-lobes are not apparent in the time domain, so this was never considered a priority until these new applications emerged.

To reduce the crosspol level, another possible improvement would be to add a dummy cable at the feed point. This would balance the cable that already comes down the feed arm. Such a cable would add symmetry to the design, which should reduce the crosspol fields. Another option for reducing the crosspol level is to add a central ground plane to the plane of symmetry. This will tend to short out the crosspol field in the aperture. These concepts will be tested in a future project.

VIII. Conclusions

We built and tested eighteen-inch diameter versions of an IRA and PRAE. Testing took place at both a time domain antenna range of Farr Research, and at the frequency domain range of Mission Research. Good correlation between the data was proved.

The narrow beam and broad pattern of the IRA is apparently useful for both spotlight mode SAR and for various applications involving remote target identification. Much work needs to be done to design a system that includes the new antenna, but the advantages seem clear. Improvements in IRAs are needed for mechanical stability, and for side-lobe reduction. There are obvious approaches available to us to remedy these problems.

There is a gap in antenna technology that the IRA can fill. If a broadband antenna is required to operate between 100 MHz and 10 GHz, then the IRA is one of very few antennas that can potentially meet the requirement. Other antennas, such as TEM horns have the bandwidth, but they have a size and shape that is generally less suitable for many applications. For these reasons, the IRA is a likely candidate for spotlight-mode SAR and remote target identification systems.

References

1. C. E. Baum, Antennas on Airplanes, Sensor and Simulation Note 435, March 1999.

2. C. E. Baum, E. G. Farr, and C. A. Frost, Transient Gain of Antennas Related to the Traditional Continuous-Wave (CW) Definition of Gain, Sensor and Simulation Note 412, July 1997.

3. E. G. Farr, C. E. Baum, and W. D. Prather, Multifunction Impulse Radiating Antennas: Theory and Experiment, Sensor and Simulation Note 413, November 1997.

4. L. H. Bowen and E. G. Farr, Recent Enhancements to the Multifunction IRA and TEM Sensors, Sensor and Simulation Note 434, February 1999.

5. John S. Gwynne. "The Propagation and Scattering Characteristics of a Forest as Measured by Coherent Ultra-Wideband Foliage Penetration SAR". Ph.D. thesis, The Ohio State University, Columbus, Ohio 43212, 1998.

6. John S. Gwynne and Glen R. Salo. "Antenna System for Unmanned Aerial Vehicles, Task 1 Report, Candidate Designs and Scale Model Summary". Mission Research Corporation, Phase II SBIR Technical Report for topic number A96-017, Mission Research Corporation, Dayton, Ohio, 1999.

7. John S. Gwynne and Jonathan D. Young, "Time Domain Characterization of UWB Antennas", presented at AMTA 14th Annual Meeting and Symposium, Columbus, Ohio, pp. 3-8, Oct. 19-23, 1992.

8. John S. Gwynne and Jonathan D. Young. "Normalized Transient Pattern Functions of Ultra-Wideband Antenna," to appear shortly in *IEEE Transactions on Antennas and Propagation*..

9. Jonathan D. Young and John S. Gwynne. "Report on Antenna Transient Patterns". Technical Report 732169-2, The Ohio State University, ElectroScience Laboratory, Columbus, Ohio 43212, 1997.

10. L. Carin, R. Kapoor, and C. E. Baum, Polarimetric SAR Imaging of Buried Landmines, *IEEE Trans. Geoscience and Remote Sensing*, Vol. 36, November 1998, pp. 1985-88.

11. J. McCorkle, *et al*, Transient Synthetic Aperture Radar and the Extraction of Anisotropic and Natural Frequency Information, Chapter 12 in *Detection and Identification of Visually Obscured Targets*, Carl E. Baum (ed.), Taylor and Francis, 1999.